



Droplet nucleation: Physically-based parameterizations and comparative evaluation

Steven J. Ghan¹, Hayder Abdul-Razzak², Athanasios Nenes³, Yi Ming⁴, Xiaohong Liu¹, Mikhail Ovchinnikov¹, Ben Shipway⁵, Nicholas Meskhidze⁶, Jun Xu^{6,7} and Xiangjun Shi^{1,8}

¹ Atmospheric and Global Change Division, Pacific Northwest National Laboratory, PO Box 999, Richland, WA 99352, USA.

² Department of Mechanical Engineering, Texas A & M University-Kingsville, MSC 191, 700 University Blvd., Kingsville, TX 78363, USA.

³ School of Earth and Atmospheric Sciences, Georgia Institute of Technology, 311 Ferst Dr., Atlanta, GA 30332-0340, USA.

⁴ Geophysical Fluid Dynamics Laboratory, PO Box 308, Princeton, NJ 08542, USA.

⁵ Met Office, FitzRoy Road, Exeter EX1 3PB, UK.

⁶ Department of Marine, Earth, and Atmospheric Sciences, North Carolina State University, 2800 Faucette Dr., Raleigh, NC 27695-8208, USA.

⁷ Chinese Research Academy of Environment Sciences, Beijing, China.

⁸ Institute of Atmospheric Physics, Chinese Academy of Sciences, Beijing, China.

Manuscript submitted 07 April 2011

One of the greatest sources of uncertainty in simulations of climate and climate change is the influence of aerosols on the optical properties of clouds. The root of this influence is the droplet nucleation process, which involves the spontaneous growth of aerosol into cloud droplets at cloud edges, during the early stages of cloud formation, and in some cases within the interior of mature clouds. Numerical models of droplet nucleation represent much of the complexity of the process, but at a computational cost that limits their application to simulations of hours or days. Physically-based parameterizations of droplet nucleation are designed to quickly estimate the number nucleated as a function of the primary controlling parameters: the aerosol number size distribution, hygroscopicity and cooling rate. Here we compare and contrast the key assumptions used in developing each of the most popular parameterizations and compare their performances under a variety of conditions. We find that the more complex parameterizations perform well under a wider variety of nucleation conditions, but all parameterizations perform well under the most common conditions. We then discuss the various applications of the parameterizations to cloud-resolving, regional and global models to study aerosol effects on clouds at a wide range of spatial and temporal scales. We compare estimates of anthropogenic aerosol indirect effects using two different parameterizations applied to the same global climate model, and find that the estimates of indirect effects differ by only 10%. We conclude with a summary of the outstanding challenges remaining for further development and application.

DOI:10.1029/2011MS000074

1. Introduction

One of the greatest sources of uncertainty in projections of future climate change is the influence of anthropogenic aerosol on the optical properties of clouds [Forster *et al.*, 2007]. By serving as the seeds (Cloud Condensation Nuclei, CCN) of cloud droplets, anthropogenic aerosol particles can increase droplet number concentration, thereby increasing total droplet surface area and hence cloud albedo if liquid water content is not changed [Twomey, 1974, 1977]. By reducing mean droplet size, drizzle production can be

inhibited under certain conditions, leading to increased liquid water content, further enhancing cloud albedo [Albrecht, 1989]. These and other mechanisms by which aerosols affect clouds and climate through their influence on droplet number are referred to collectively as the aerosol

To whom correspondence should be addressed.

Steven J. Ghan, Atmospheric and Global Change Division, Pacific Northwest National Laboratory, PO Box 999, Richland, WA 99352, USA. steve.ghan@pnl.gov

indirect effect on climate [Haywood and Boucher, 2000; Lohmann and Feichter, 2005; Stevens and Feingold, 2009].

The root of this influence is the droplet nucleation process. Droplet nucleation involves the simultaneous condensational growth of an aerosol population in a cooling air parcel until maximum supersaturation is achieved and some of the wet particles are large enough to grow spontaneously into cloud droplets. Droplet nucleation also has important effects on the aerosol population, as nucleation scavenging of aerosol particles (i.e., when particles activated to form cloud droplets are subsequently removed from the atmosphere by precipitation from the cloud) is the dominant removal mechanism for accumulation mode (0.05–0.2 micron radius) aerosol [Jensen and Charlson, 1984; Flossmann et al., 1985]. In addition, aqueous phase oxidation of sulfur in cloud droplets is a major source of sulfate after particles are activated when droplets form and are then subsequently resuspended when cloud droplets evaporate [Hoppel et al., 1986; Meng and Seinfeld, 1994; Rasch et al., 2000]. Similarly, recent work [Sorooshian et al., 2007; Ervens et al., 2008; Perri et al., 2009] suggests that aqueous phase chemistry in cloud droplets is also an important source of secondary organic aerosol. The activation process determines which particles gain sulfate and organic matter within cloud droplets.

The first attempts to represent droplet nucleation in climate models [Jones et al., 1994; Jones and Slingo, 1996; Lohmann and Feichter, 1997] relied on empirical relationships between droplet number and measures of the aerosol such as sulfate mass concentration [Leaith et al., 1992; Leaith and Isaac, 1994; Boucher and Lohmann, 1995] or aerosol number [Jones et al., 1994; Martin et al., 1994]. These relationships do not account for the dependence of the droplet nucleation on size distribution, composition, or updraft velocity, and hence are extremely limited in their applicability to the wide variety of conditions controlling droplet formation.

Recognition of these limitations has driven the development of physically-based schemes that can more completely represent the dependence of the process on all of the key controlling parameters. These schemes have the added benefit of diagnosing the maximum supersaturation in updrafts and the partitioning of the aerosol into cloud-borne and interstitial phases so that aqueous phase chemistry and nucleation scavenging can be represented more realistically.

The theory of droplet nucleation is founded on seminal work by Köhler [1921, 1926], who determined the equilibrium radius r of particles as a function of dry radius r_d and relative humidity RH . For supersaturated conditions the wet size generally dominates the dry size and the Köhler equilibrium can be approximated in terms of supersaturation S (defined as RH) as [Seinfeld and Pandis, 1998]

$$S_{eq} = \frac{A}{r} - \frac{\kappa r_d^3}{r^3} \quad (1)$$

where the Kelvin coefficient A and hygroscopicity parameter κ are defined in Appendix A. Solutions to equation (1) for ammonium sulfate particles of four different dry radii are illustrated in Figure 1. For each dry particle size there is a maximum supersaturation in equilibrium with the wet radius. The maximum supersaturation is called the critical supersaturation S_c for the particle, because under most ambient conditions if the supersaturation in a cooling air parcel exceeds S_c the particle radius will grow beyond the equilibrium size at the maximum supersaturation, and the particles will continue to grow spontaneously until the supersaturation is reduced to a value at or below equilibrium. The critical supersaturation can be found by solving for the maximum of equation (1),

$$S_c \equiv \left(\frac{4A^3}{27\kappa r_d^3} \right)^{1/2} \quad (2)$$

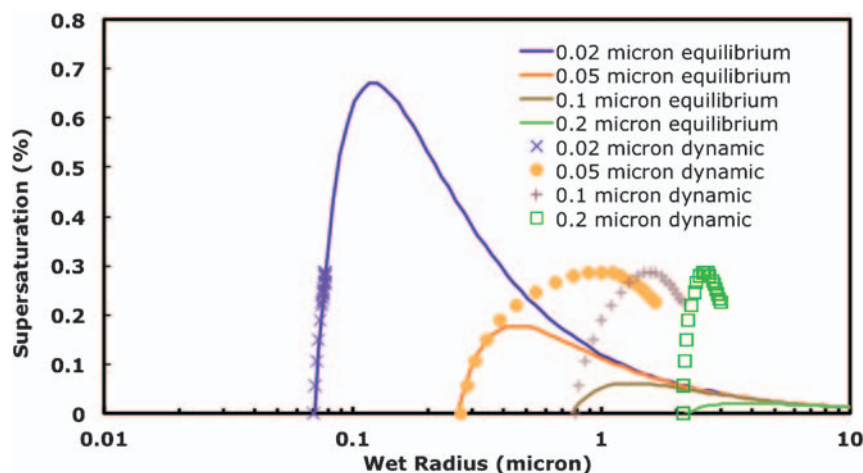


Figure 1. Supersaturation as a function of equilibrium wet radius (solid curves) and the wet radius every 1 s for a rising air parcel (individual points) according to dynamic Köhler theory for ammonium sulfate particles with four different dry radii.

and the critical radius r_c for activating particles (corresponding to the equilibrium wet size at the maxima of the Köhler curve for the particle) can be written

$$r_c \equiv \left(\frac{3kr_d^3}{A} \right)^{1/2}. \quad (3)$$

The equilibrium theory can determine which particles form droplets in an air parcel if its supersaturation history is known. The latter requires knowledge of the aerosol size distribution and the dynamical forcing (mixing, radiative or expansion cooling) that generates supersaturation; this is addressed with the more general dynamic Köhler theory [Pruppacher and Klett, 1997; Seinfeld and Pandis, 1998]. This theory consists of equations for the mass balance of each particle j and the supersaturation balance of the air parcel, which under the assumptions of adiabaticity (no exchange of mass or enthalpy with the environment - this simplification will be addressed in section 2) and expansion cooling can be expressed as [Howell, 1949]

$$\frac{dr_j}{dt} = \frac{G}{r_j} \left(S - \frac{A}{r_j} + \frac{\kappa r_{dj}^3}{r_j^3} \right) \quad (4)$$

$$\frac{dS}{dt} = \alpha w - \gamma \frac{dW}{dt} \quad (5)$$

where the growth coefficient G and the coefficients α and γ , which are weak functions of temperature and pressure, are defined in Appendix A, w is the updraft velocity, and the condensation rate can be expressed in terms of the growth rate of all particles,

$$\frac{dW}{dt} = \frac{4\pi\rho_w}{\rho_a V} \sum_j r_j^2 \frac{dr_j}{dt} \quad (6)$$

where W is the liquid water mass mixing ratio, ρ_a is the density of air and the sum is over all particles in a parcel of volume V large enough to contain a representative number of particles but small enough that the updraft velocity can be considered uniform within the parcel. Note that (1) is simply the equilibrium form of (4). Although the effect of the cooling rate on supersaturation in (5) is expressed in terms of updraft velocity, Ghan *et al.* [1993] show that it can be expressed more generally to account for radiative cooling as well.

A key parameter controlling the nucleation process is the updraft velocity. In cloud-resolving models the grid is fine enough to explicitly resolve spatial variability in the updraft velocity, but in large-scale models (with grid cells much larger than the 100 m size of turbulent eddies in the boundary layer), it is important to account for the subgrid variability and its influence on droplet nucleation. This issue is addressed in section 4.

According to (5) and (6) the supersaturation history depends on the history of the updraft velocity and the

growth of all particles. Each particle competes with all others for water, with condensation on each particle affecting the supersaturation according to (5) and hence the growth of all particles according to (4). The complexity of the coupled equations (4)–(6) makes analytic solution impossible without approximations.

Numerical models of droplet nucleation are capable of representing much of the complexity of the process. Most numerical models [Warner, 1973; Fitzgerald, 1974; Jensen and Charlson, 1984; Flossmann *et al.*, 1985; Abdul-Razzak *et al.*, 1998; Nenes *et al.*, 2001] represent the aerosol in terms of a large number (order 100) of sections of the size distribution, with each section assumed to be composed of an internal mixture of identical particles with the same size and composition. Equation (6) then becomes

$$\frac{dW}{dt} = \frac{4\pi\rho_w}{\rho_a} \sum_i N_i r_i^2 \frac{dr_i}{dt} \quad (7)$$

where N_i is the number concentration of particles in section i . More general formulations [Russell and Seinfeld, 1998] represent the aerosol in terms of sections with multiple externally-mixed populations. Particle-resolved representations of the aerosol [Andrejczuk *et al.*, 2008; Shima *et al.*, 2009] have also been applied to the droplet nucleation process using (6) rather than (7).

Figure 2 shows a numerical simulation of supersaturation for a rising air parcel. Initially the supersaturation rises as supersaturation production by adiabatic cooling (the αw term in equation (5)) dominates supersaturation loss by condensation on droplets and unactivated aerosol (the $-\gamma \frac{dW}{dt}$ term in equation (5)). As the particles grow their

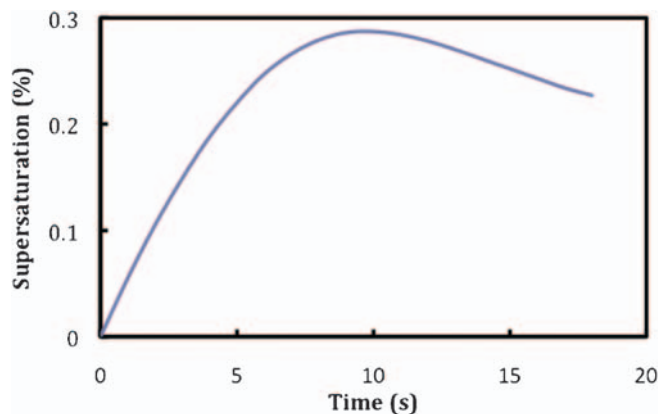


Figure 2. Numerical solution for supersaturation in an air parcel rising at a rate of 1 m s^{-1} with a lognormal size distribution of ammonium sulfate aerosol with total number concentration 1000 cm^{-3} , number mode radius $0.05 \text{ }\mu\text{m}$, and geometric standard deviation 2. At time zero the aerosol is assumed to be in equilibrium with a 100% relative humidity. A total of 144 sections were used with size ranges such that an equal number of particles are in each section, with the middle section corresponding to the number mode radius.

surface area increases, which together with a rise in supersaturation increases the condensation rate. Eventually (here, after 10 s) droplets grow large enough and supersaturation becomes great enough that the condensation rate exceeds supersaturation production, and the parcel supersaturation begins to decrease.

According to equilibrium Köhler theory a particle remains in equilibrium with parcel supersaturation while $S < S_c$ and instantaneously activates when $S \geq S_c$. Although this often is a good approximation of particle behavior, it does not always hold. Characteristic examples of the dynamical behavior of four different particle sizes for this case are illustrated in Figure 1. Initially all four particle sizes grow, but the inertial kinetic limitation mechanism [Nenes *et al.*, 2001] limits the growth of the larger particles to sizes smaller than expected from equilibrium Köhler theory. According to equation (4) this lag in growth actually enhances condensation as the supersaturation exceeds the equilibrium supersaturation for the particle size. Although the growth of the smallest of the four particle sizes (dry radius 0.02 μm) follows equilibrium Köhler theory, the supersaturation of the air parcel never exceeds the critical supersaturation for that particle size, so those particles lose water when the supersaturation declines. In contrast, the larger particles exceed their critical size and hence continue to grow beyond the point of maximum supersaturation. Thus, the activation process separates the aerosol into a population that forms cloud droplets and the remainder that do not (often referred to as interstitial aerosol). The smallest of those that form droplets typically activate last in the cloud parcel, as they have a critical supersaturation close to the parcel maximum supersaturation; larger particles have a lower S_c , are activated sooner and grow beyond their critical size before maximum supersaturation occurs. The largest particles are typically subject to the inertial kinetic limitation mechanism, during which r_c is not attained before maximum supersaturation is achieved (e.g., dry radius 0.2 μm in Figure 1). Although not strictly activated, these inertially-limited particles are indistinguishable from activated droplets, because they exhibit comparable sizes and continue to grow (as their S_{eq} is very small). The time for which $S > S_c$ may be insufficient for particles with $S_c \sim S_{max}$ to grow beyond their r_c and activate; slightly larger particles may initially activate, but subsequently deactivate because S may drop below S_{eq} and evaporate the particle. Both of these kinetic limitation mechanisms (identified by Nenes *et al.* [2001] as the deactivation and evaporation mechanisms, respectively) appreciably affect droplet number under highly polluted conditions [Nenes *et al.*, 2001]. For all other atmospherically-relevant conditions, it is sufficient to state that particles for which $S_c \leq S_{max}$ will nucleate cloud droplets.

Numerical models of droplet nucleation are computationally expensive, because of the need to discretize the aerosol size distribution, resolve the short time scales of the

condensation process, and integrate over time until maximum supersaturation is achieved. This limits their application to exploration of parameter space with parcel models or to simulations of hours to days with three-dimensional models [Kogan, 1991; Khairoutdinov and Kogan, 1999]. Even for such short simulations there are challenges due to discretization errors in Eulerian representations of water and temperature transport and the nonlinear dependence of supersaturation on temperature and water vapor [Clark, 1974; Stevens *et al.*, 1996; Morrison and Grabowski, 2008]. This concern has led to the development of a Lagrangian particle-based representation of the aerosol and cloud droplets [Andrejczuk *et al.*, 2008, 2010], but at a considerable computational expense. Thus, although numerical models provide valuable benchmark simulations of the nucleation process and can be used in short cloud simulations, they are not practical for global simulations of decades or centuries.

Physically-based parameterizations of droplet nucleation are designed to quickly diagnose the number nucleated as a function of the primary controlling parameters: the cooling rate and the size distribution of aerosol number and hygroscopicity. This permits treatment of droplet nucleation for a spectrum of updraft velocities within each grid cell in long global simulations [Ghan *et al.*, 1997]. Thus, parameterizations have been widely used in global models to estimate aerosol indirect effects, and will be relied on for future multi-century simulations of climate change.

In this review article we compare and contrast the key assumptions and approximations used in developing each of the most popular parameterizations and compare their performances under a variety of conditions. The parameterizations are summarized in Table 1. We then discuss the various applications of the parameterizations to cloud-resolving, regional and global models to study aerosol effects on clouds at a wide range of spatial and temporal scales, and compare estimates of anthropogenic aerosol indirect effects with two parameterizations applied to the same model. We conclude with a summary of the outstanding challenges remaining for further development.

2. Parameterization Descriptions

Given the fact that the equilibrium Köhler theory accurately diagnoses activation of particles provided the maximum supersaturation is known, the crux of the parameterization problem is the determination of the maximum supersaturation in a cloudy parcel. However, equations (4)–(6) are too complex for analytic solutions without approximations. Most parameterizations therefore rely on the following assumptions.

1. No cloud droplets are present before cooling begins. Although ice crystals might be present, we assume their influence on supersaturation is too slow to affect aerosol activation.
2. Adiabatic conditions.

Table 1. Comparison of Features of Aerosol Activation Schemes

Scheme and Key Reference	Mass Transfer	Condensation Coefficient	Integration Over Size Distribution	Iterative Solution	Kinetic Limitations
Abdul-Razzak <i>Abdul-Razzak and Ghan [2000]</i>	scaling of G	scaling of G	analytic	no	neglected
Nenes <i>Fountoukis and Nenes [2005]</i>	explicit	explicit dependence	analytic	yes	treated
Ming <i>Ming et al. [2006]</i>	explicit	explicit dependence	numerical	yes	empirical
Hänel <i>Hänel [1987]</i>	constant G	fixed	numerical	yes	neglected
Cohard <i>Cohard et al. [2000]</i>	constant G	undefined	analytic	no	neglected
Khvorostyanov <i>Khvorostyanov and Curry [2009]</i>	explicit	explicit dependence	analytic	no	neglected
Shipway <i>Shipway and Abel [2010]</i>	explicit	explicit dependence	analytic	yes	treated
Kivekas <i>Kivekas et al. [2008]</i>	empirical	fixed	analytic	no	empirical

3. The aerosol population can be represented in terms of the distribution of number with size, which can be described by a power law, by multiple sections, or by lognormal modes, each with a uniform bulk hygroscopicity.
4. Particles are composed of internal mixtures of salts and insoluble components within each section or mode.
5. The volume of particle water at maximum supersaturation is substantially larger than the dry aerosol volume.
6. The number of nucleated droplets is determined by the number of particles with critical supersaturation less than the maximum supersaturation.
7. Particles grow in equilibrium with relative humidity until the supersaturation exceeds the particle critical value for activation.
8. Beyond the point of activation, particle growth rates are not significantly influenced by droplet curvature and solute effects.

Some of these approximations have been relaxed in a few parameterizations.

Assumption 1 restricts the theory to droplets forming near the base of existing clouds or as a result of adiabatic or diabatic cooling in clear air. Thus, the condensation rate can be expressed in terms of droplets forming on the aerosol in the cooling air parcel. In section 6 we will address the case of droplet formation within the interior of existing clouds.

Assumption 2 was used in equation (5). *Mason and Chien [1962]* and *Warner [1973]* first explored the influence of entrainment. *Barahona and Nenes [2007]* have relaxed this assumption and shown that a more general treatment can account for the influence of entrainment provided the entrainment rate is known.

Under assumption 3, the aerosol size distribution is approximated in terms of a power law [*Twomey, 1959*],

$$\frac{dN}{dr_d} = ar_d^{-b} \quad (8)$$

multiple sections [*Abdul-Razzak and Ghan, 2002; Nenes and Seinfeld, 2003; Ming et al., 2006*],

$$\frac{dN}{dr_d} = \frac{N_i}{r_i - r_{i-1}} \quad (9)$$

or multiple lognormal distributions [*Abdul-Razzak and Ghan, 2000; Fountoukis and Nenes, 2005*],

$$\frac{dN}{d \ln r_d} = \sum_m \frac{N_m}{\sqrt{2\pi \ln \sigma_m}} \exp\left(-\frac{\ln^2(r_d/r_m)}{2 \ln^2 \sigma_m}\right) \quad (10)$$

where a and b are constants defining the size distribution, N_i is the number concentration in section i , r_i is the dry radius at the upper boundary of section i , N_m is the number concentration in mode m , and r_m and σ_m are the mode radius and geometric standard deviation for mode m . If the wet radius of the particle and its growth rate are known then the condensation rate can be expressed in terms of the size distribution,

$$\frac{dW}{dt} = \frac{4\pi\rho_w}{\rho_a} \int_0^\infty r^2 \frac{dN}{dr_d} \frac{dr}{dt} dr_d. \quad (11)$$

It is helpful to express the aerosol number distribution with size in terms of critical supersaturation,

$$\frac{dN}{d \ln S_c} = \frac{dN}{d \ln r_d} \frac{d \ln r_d}{d \ln S_c}. \quad (12)$$

Noting that from (2)

$$\frac{d \ln r_d}{d \ln S_c} = -\frac{2}{3} \quad (13)$$

equations (8)–(11) become

$$\frac{dN}{dS_c} = -\frac{2a}{3S_c} \left(\frac{4A^3}{27kS_c^2}\right)^{\frac{1-b}{3}} \quad (14)$$

$$\frac{dN}{dS_c} = \frac{N_i}{S_i - S_{i-1}} \quad (15)$$

$$\frac{dN}{d \ln S_c} = - \sum_m \frac{2N_m}{3\sqrt{2\pi} \ln \sigma_m} \exp\left(-\frac{\ln^2(S_m/S_c)^{2/3}}{2 \ln^2 \sigma_m}\right) \quad (16)$$

$$\frac{dW}{dt} = \frac{4\pi\rho_w}{\rho_a} \int_0^\infty r^2 \frac{dN}{dS_c} \frac{dr}{dt} dS_c \quad (17)$$

where S_i denotes the critical supersaturation at the boundary of bin i and S_m is the critical supersaturation for the mode radius of mode m . Then if the maximum supersaturation S_{max} is known, the number nucleated can be determined by integrating (14)–(16) from zero to S_{max} , yielding

$$N_{act} = cS_{max}^k \quad (18)$$

$$N_{act} = \sum_{j=1}^{i-1} N_j + N_j \frac{S_{max} - S_i}{S_{i+1} - S_i} \quad (19)$$

$$N_{act} = \frac{1}{2} \sum_M N_m [1 - \text{erf}(z_m)] \quad (20)$$

where

$$k \equiv \frac{2}{3}(b-1) \quad (21)$$

$$z_m \equiv 2 \ln(S_m/S_{max}) / (3\sqrt{2} \ln \sigma_m). \quad (22)$$

A useful approximation to (20) is to replace the error function $\text{erf}(z)$ with the hyperbolic tangent $\tanh(2z/\pi)$ [Ghan *et al.*, 1993; Khvorostyanov and Curry, 2006], so that (20) becomes

$$N_{act} = \sum_m \frac{N_m}{1 + (S_m/S_{max})^{c_m}} \quad (23)$$

where $c_m \equiv 9/(3\sqrt{2\pi} \ln \sigma_m)$. The distribution of number with supersaturation that is consistent with (23) can be written [Khvorostyanov and Curry, 2006]

$$\frac{dN}{dS_c} = \sum_m \frac{c_m N_m S_c^{c_m}}{S_m^{1+c_m}} / \left[1 + (S_c/S_m)^{c_m}\right]^2 \quad (24)$$

For small S_c with respect to S_m , (24) reduces to a sum of multiple power laws. For the more general case (24) is a multimode version of the extension of the power law size distribution proposed for a single mode by Cohard *et al.* [1998, 2000] and extended to the multimode case by Shipway and Abel [2010]. This provides a connection between parameterizations based on log-normal size distributions and those based on power laws. In addition, (23) is much faster to compute than the error function in (20), and

is a good approximation under most conditions [Ghan *et al.*, 1993; Khvorostyanov and Curry, 2006].

Under assumption 4, the hygroscopicity of each section or mode is given by the volume mean of the hygroscopicity of the components comprising the section or mode, as described in Appendix A.

Assumption 5 has already been invoked in equation (1). In addition, as we shall see later this assumption simplifies the treatment of the effects of surfactants on droplet nucleation.

Assumption 6 permits the number activated to be determined from the CCN spectrum and the maximum supersaturation, thus reducing the problem to that of determining the maximum supersaturation. This assumption neglects kinetic limitation mechanisms for droplet nucleation. As noted earlier, such an approximation performs well for all but extremely polluted conditions.

Assumption 7 applies an equilibrium growth approximation to determine the droplet size distribution at maximum supersaturation. This is a critical step in determining the maximum supersaturation. To see this, consider the combination of equations (5) and (17) at maximum supersaturation:

$$\alpha w = \gamma^* \int_0^{S_{max}} r^2 \frac{dN}{dS_c} \frac{dr}{dt} dS_c \quad (25)$$

where

$$\gamma^* \equiv \frac{4\pi\rho_w\gamma}{\rho_a}$$

and the upper limit of the integral is S_{max} because no particles with $S_c > S_{max}$ can be activated.

The path forward is to use equation (25) to determine S_{max} . To do so the radius and its growth must be related to S_{max} . Assumption 7 can be used in combination with equations (1) and (4) to do this. First write equation (4) as

$$\frac{dr}{dt} = \frac{G}{r} (S - S_{eq}). \quad (26)$$

where S_{eq} is given by (1). We apply assumption 7 to (26) and integrate from the time of activation t_{act} to the time of maximum supersaturation t_{max} :

$$r^2(t_{max}) = r^2(t_{act}) + 2G \int_{t_{act}}^{t_{max}} (S - S_{eq}) dt \quad (27)$$

where $r^2(t_{act})$ is often assumed to be given by (3). Note that according to Figure 1, assumption 6 is not appropriate for larger particles, specifically for particles with radius 0.1 μm or larger for the conditions of Figure 1.

Assumption 8 neglects S_{eq} in (26) and (27). Then (26) at maximum supersaturation and (27) become

$$r \frac{dr}{dt} = GS_{\max} \quad (28)$$

$$r^2(t_{\max}) = r^2(t_{act}) + 2G \int_{t_{act}}^{t_{\max}} S dt. \quad (29)$$

As is evident in Figure 1, assumption 8 is a reasonable approximation for particles that activate well before maximum supersaturation, but not for particles that activate just before maximum supersaturation. Thus, (28) may overestimate the growth rate of particles with S_c near S_{\max} . However, unless inertial kinetic limitations are important [Barahona et al., 2010], (29) still accurately determines the droplet size at t_{\max} because t_{act} is near t_{\max} for those particles.

Substituting (28) and (29) into (25) yields

$$\alpha w = \gamma^* GS_{\max} \int_0^{S_{\max}} \left(r^2(t_{act}) + 2G \int_{t_{act}}^{t_{\max}} S dt \right)^{1/2} \frac{dN}{dS_c} dS_c \quad (30)$$

Solution of (30) is facilitated by splitting the aerosol population into two parts [Nenes and Seinfeld, 2003]: (a) particles with S_c near S_{\max} such that

$$r^2(t_{act}) \gg 2G \int_{t_{act}}^{t_{\max}} S dt \quad (31)$$

and (b), particles with S_c much less than S_{\max} , such that

$$r^2(t_{act}) \ll 2G \int_{t_{act}}^{t_{\max}} S dt \quad (32)$$

Then (30) can be reduced to

$$\alpha w = \gamma^* GS_{\max} \left[\int_0^{S_{part}} \left(2G \int_{t_{act}}^{t_{\max}} S dt \right)^{1/2} \frac{dN}{dS_c} dS_c + \int_{S_{part}}^{S_{\max}} r(t_{act}) \frac{dN}{dS_c} dS_c \right] \quad (33)$$

where S_{part} is a partitioning supersaturation [Nenes and Seinfeld, 2003] that distinguishes between particles that grow substantially between t_{act} and t_{\max} , and those that do not.

We are now prepared to distinguish between the various different parameterizations of droplet nucleation.

The first parameterization of droplet nucleation was formulated by Twomey [1959]. Twomey's scheme assumes $S_{part} = S_{\max}$ so that the second term in (33) is neglected. This underestimates the size of particles with S_c near S_{\max} , but the growth rate of those particles should be slow according to (26). Twomey assumes a power law for the

CCN spectrum (i.e., equation (18)). By approximating the integral of supersaturation in (33) in terms of S_{\max}

$$\int_{t_{act}}^{t_{\max}} S dt \cong \frac{S_{\max}^2 - S_c^2}{2\alpha w} \quad (34)$$

Twomey is able to solve (33) for S_{\max} in terms of w and the parameters of the CCN spectrum. However, Twomey's solution is unbounded at high updraft velocity, and hence produces unphysical results (droplet number exceeding aerosol number) for large updraft velocity or low aerosol concentrations [Ghan et al., 1993]. Cohard et al. [1998, 2000] have extended the Twomey solution by replacing the power law size distribution with a more general expression that limits the number activated at high supersaturation. Shipway and Abel [2010] extended that solution to the multimode case.

The second term in (33) was introduced by Ghan et al. [1993], who assumed $S_{part} = 0$ so that the first term is neglected and when $S = S_{\max}$ the particles are at their critical size for activation. Thus, under some conditions droplet size is underestimated for particles that grow after their radius reaches r_c , i.e., particles with $S_c \ll S_{\max}$. However, as is evident from Figure 1, growth of the larger droplets does not follow their Köhler curves, and their size at maximum supersaturation is not far from their critical size for activation. Ghan et al. [1993] also departed from Twomey by retaining S_{eq} in (26), and by assuming a single lognormal aerosol size distribution. The integrals in (33) are then performed analytically, and the resulting function of S_{\max} is approximated to permit a simple analytic expression for the number activated: $N_{act} = wN_a / (w + dN_a)$ where the parameter d depends on the width of the aerosol size distribution. Ghan et al. [1995] extended the scheme to the case of multiple lognormal size distributions. Chuang et al. [1997] introduced empirical expressions for the parameter d to account for dependence on the updraft velocity and mean aerosol particle size. Lin and Leitch [1997] estimated the parameter d from observations.

A major weakness of the Ghan et al. [1993] scheme is that it does not account for the dependence of the number nucleated on the mean radius for each mode. Under most conditions the scheme underestimates the droplet size and hence the condensation rate, which leads it to overestimate the maximum supersaturation and the number nucleated by as much as a factor of three.

Abdul-Razzak et al. [1998] and Abdul-Razzak and Ghan [2000] combined the treatments of Twomey and Ghan et al., integrating both terms in (33) from 0 to S_{\max} but neglecting the S_{eq} term in (26), i.e., neglecting the curvature and solute terms beyond activation. This yields a complex function of S_{\max} that cannot be solved analytically. However, Abdul-Razzak et al. used numerical simulations for a single lognormal size distribution to find that the ratio S_{nl}/S_{\max} is

proportional to simple functions of S_m and two non-dimensional parameters,

$$\eta_m \equiv \frac{2(\alpha w/G)^{3/2}}{\gamma^* N_m} \quad (35)$$

$$\zeta \equiv \frac{2A}{3} \left(\frac{\alpha w}{G} \right)^{1/2} \quad (36)$$

Since neither of these parameters depends on the width of the size distribution, Abdul-Razzak et al. parameterized the dependence of S_{max} on σ from a large number of numerical solutions. The result for the multiple lognormal case [Abdul-Razzak and Ghan, 2000] is

$$S_{max}^2 = 1 / \sum_m \frac{1}{S_m^2} \left[f_m \left(\frac{\zeta}{\eta_m} \right)^{3/2} + g_m \left(\frac{S_m^2}{\eta_m + 3\zeta} \right)^{3/4} \right] \quad (37)$$

where

$$f_m \equiv 0.5 \exp(2.5 \ln^2 \sigma_m) \quad (38)$$

$$g_m \equiv 1 + 0.25 \ln \sigma_m \quad (39)$$

Although (37) diagnoses S_{max} accurately under a wide variety of conditions, it should be noted that it does not represent kinetic limitations on droplet nucleation, which can be important under highly polluted conditions [Nenes et al., 2001]. However, as we shall see, it performs surprisingly well under many conditions.

Note also that the Abdul-Razzak scheme is tuned to numerical simulations using a particular value (1.0) of the condensation coefficient α_c that is used to determine G (see Appendix A), and that G in (35) and (36) is estimated neglecting gas kinetic effects completely (i.e., an infinite radius in equations (A5) and (A6)). The value of α_c is uncertain to within a factor of three for pure water, and is further reduced by the presence of organic films on the particle surface [Chuang, 2003]. The treatment of G in the Abdul-Razzak scheme limits its ability to account for such variations in α_c . However, the dependence on gas kinetic effects can be added to the scheme by approximating G in (35) and (36) as

$$G = G_0 G_{ac} / G_{acl} \quad (40)$$

where G_0 is the value of G estimated without gas kinetic effects, G_{ac} is estimated using the critical radius corresponding to the number mode radius and using the selected value of the condensation coefficient, and G_{acl} is estimated using the same critical radius but a value of 1.0 for the condensation coefficient. This treatment of G yields the same results as the original tuned parameterization when the condensation coefficient equals 1.0 (and thus preserves the tuning), but as

we shall see it accounts for the dependence on the value of the condensation coefficient remarkably well.

The limitations of the Abdul-Razzak scheme were addressed by Nenes and Seinfeld [2003] for a sectional representation of the size distribution and by Fountoukis and Nenes [2005] for a lognormal representation. Considerable care was devoted to relating S_{part} to S_{max} particularly for conditions when kinetic limitations on droplet nucleation are expected. The extent of kinetic limitations is expressed in terms of the difference between S_{max}^2 and 2ζ . When kinetic limitations are expected, the relationship between S_{max} and S_{part} is determined empirically from numerical simulations for a range of conditions.

Another unique feature of the Nenes scheme is its ability to account for the influence of gas kinetics on the water vapor diffusivity. This influence depends on particle size and on the value of the condensation coefficient α_c (see Appendix A). Fountoukis and Nenes [2005] found that an average value of the diffusivity over an appropriate size range can account for the influence of gas kinetics on droplet nucleation. By expressing the solution in terms of α_c , the scheme is applicable to a range of values of the condensation coefficient. This same approach was also adopted in the Shipway and Abel [2010] scheme.

Although, unlike the Abdul-Razzak scheme, the Nenes scheme does not approximate functions of S_{max} and does not rely on empirical relationships (except when kinetic limitations are dominant throughout the CCN population), it does require iterations to solve for S_{max} . It is consequently a factor of 20–100 more computationally expensive than the Abdul-Razzak scheme, though it is still much less expensive than the full numerical integration.

Another parameterization that uses iteration is that developed by Ming et al. [2006]. Population splitting is not used; instead, the integration over S_c in equation (33) is performed numerically using a sectional representation of the aerosol size distribution. Kinetic effects are treated by using an empirical modification of (33):

$$\int_{t_{act}}^{t_{max}} S dt \cong \frac{S_{max}^{2.4} - S_c^{2.4}}{2\alpha w} \quad (41)$$

and G is evaluated at the critical radius r_c . The value 2.4 for the exponent has been determined empirically from numerical simulations that treat kinetic effects. The expression for the particle growth rate used to estimate the condensation rate retains the S_{eq} term in (26). Thus, under some conditions this scheme could be more accurate than the Nenes scheme. However, the use of numerical integration over size increases its computational cost considerably, although it is also much faster than explicit numerical integration over time.

Cohard *et al.* [1998, 2000] extended Twomey's [1959] parameterization by adding a term to the power law CCN spectrum to limit activation at high supersaturation. Khvorostyanov and Curry [2006] showed how Cohard's CCN spectrum is an approximation to that of a lognormal distribution. Although this valuable extension is limited to a single mode, Shipway and Abel [2010] recently extended it to the multimode case, related the aerosol physicochemistry to the spectrum parameters (using results of Khvorostyanov and Curry [2006]), and demonstrated agreement with numerical simulations of droplet formation to within 20%.

Several other droplet nucleation parameterizations have been proposed [Hänel, 1987; Khvorostyanov and Curry, 2008; Kivekas *et al.*, 2008; Khvorostyanov and Curry, 2009]. We will not examine them in detail, but will briefly summarize them here.

Hänel [1987] adopted some of the same assumptions later adopted by Ghan *et al.* [1993], namely that at maximum supersaturation all activated particles are at their critical size, and retains the S_{eq} term in (26). The resulting expression for supersaturation balance at maximum supersaturation

$$\alpha w = \gamma^* G \left[\int_0^{S_{max}} (S_{max} - S_c) r_c \frac{dN}{dS_c} dS_c \right] \quad (42)$$

can be rearranged in the form

$$S_{max} = \left(\frac{\alpha w}{\gamma^* G} + \int_0^{S_{max}} S_c r_c \frac{dN}{dS_c} dS_c \right) / \int_0^{S_{max}} r_c \frac{dN}{dS_c} dS_c \quad (43)$$

Equation (43) can be solved by numerical integration over size and by iteration on S_{max} in a manner similar to that of Ming *et al.* Errors in (43) due to the assumption that $r(t_{max}) = r_c$ are addressed by introducing an empirical correction factor based on numerical simulations with a parcel model. Roelofs *et al.* [2006] have applied this scheme to the ECHAM5-HAM global climate model.

Khvorostyanov and Curry [2008, 2009] use (23) to approximate the number nucleated as a function of S_{max} . This simplifies the solution for S_{max} via a quick numerical solution for the time of maximum supersaturation. Comparisons of the number nucleated with numerical integrations indicate agreement to within 10% for a modest range of conditions. So far the scheme has been limited to the case of a single lognormal aerosol mode.

Kivekas *et al.* [2008] use a large number of numerical simulations to parameterize the size of the smallest particle activated in terms of a simple function of updraft velocity, total submicron volume concentration, the soluble volume fraction, and a number to volume ratio, where the number is for particles larger than a cutoff radius (0.05 μm) and the volume is the total submicron aerosol volume. The total number nucleated can then be estimated from the number of particles larger than the smallest size activated. The

scheme determines the number nucleated to within 15% for a range of conditions and is exceptionally fast.

Several extensions to the conditions considered above have also been introduced. Barahona and Nenes [2007] showed that the influence of entrainment on supersaturation and activation can be accounted for by generalizing the expression for the adiabatic expansion parameter α in (5):

$$\alpha \equiv \left(\frac{gM_w L}{c_p R T^2} - \frac{gM_a}{RT} \right) \left(1 - \frac{e}{e_c} \right) \quad (44)$$

where e is the entrainment rate (m^{-1}) and e_c is the critical entrainment rate (defined as the value of e that completely inhibits cloud formation), given by

$$e_c \equiv \frac{\frac{gM_w L}{c_p R T^2} - \frac{gM_a}{RT}}{(1 - RH) - \frac{M_w L}{RT^2} (T - T')} \quad (45)$$

where T^* and RH are the temperature and relative humidity of the cloud environment. Thus, if $e > e_c$ then $\alpha < 0$ and droplets do not nucleate. This treatment of the dependence of activation on entrainment can be applied to any physically-based parameterization that explicitly considers the cooling rate term αw in (5). Although it provides a simple treatment of the effects of entrainment on supersaturation in clouds, it does not address the potential effects of activation of aerosol entrained into the cloud from the lateral edges of the cloud [Fridlind *et al.*, 2004].

A second extension is treatment of the influence of organic surfactants on the activation process. Organic surfactants lower the surface tension of the particle, which according to equation (2) reduces the critical supersaturation of the particle. But most organic surfactants have a lower hygroscopicity than that of sea salt and sulfate, which reduces the bulk hygroscopicity of the particle and hence increases the critical supersaturation. Thus, the net effect depends on the hygroscopicity of the surfactant and how strongly it influences surface tension.

The effects of organic surfactants on aerosol activation has been addressed by Abdul-Razzak and Ghan [2004]. They showed that, if the surface tension can be expressed analytically in terms of the surfactant concentration (which changes through dilution as the particle grows by condensation of water) then surfactant effects can be quantified using the surface tension estimated at the critical size corresponding to the number mode radius of the size distribution. In this case the expression for the critical radius must be generalized to account for the dependence of surface tension (and the parameter A that depends on surface tension – see the Appendix) on the wet radius:

$$r_c^4 \frac{dS}{dr_c} = A r_c^2 - 3k r_m^3 - r_c^3 \frac{dA}{dr_c} = 0 \quad (46)$$

Equation (46) can be solved for r_c by iteration with the expression for the dependence of surface tension on surfactant concentration and hence r_c . Once r_c is known, the parameter A can be calculated and the expression for the critical supersaturation for the mode radius, S_{mp} can be evaluated and used in (37) to diagnose S_{max} . The number activated follows from (20).

Rissman et al. [2004] also extended the Abdul-Razzak scheme to include surface tension effects consistent with Köhler theory, using a formalism similar to equation (46); a simplified explicit form was then derived and subsequently used to compute analytical sensitivities of nucleated droplet number to chemical, dynamical and microphysical parameters. The parameterization frameworks of *Nenes and Seinfeld* [2003] and *Ming et al.* [2006] can also directly account for organic surfactant impacts on droplet formation, provided the routines used to compute the critical supersaturation spectrum (equation (5)) consider surface tension impacts (e.g., equation (46)). *Nenes and Seinfeld* [2003] demonstrate this capability by using surface tension data derived from Po Valley fogwater; a global modeling study on surface-tension impacts on cloud droplet number has not been carried out to date.

If giant CCN are present then *Barahona et al.* [2010] have shown that it is important to include an additional condensation rate term that accounts for condensation on inertia-limited large particles.

An alternative to parameterizations is the use of look-up tables based on a large number of numerical simulations. To reduce the dimensionality of the look-up table, *Saleeby and Cotton* [2004] accounted for the dependence on only four parameters: temperature, updraft velocity, CCN concentration, and median radius of the CCN size distribution. *Segal and Khain* [2006] tabulated droplet number for several combinations of updraft velocity, CCN concentration, median radius, and width of the size distribution. Such treatments can be computationally very fast and are appropriate for conditions when the composition and number of modes are uniform, but for global applications, which span a wide range of composition and size distributions, additional dimensions are required because, as we shall see, droplet nucleation depends on many parameters. Although look-up tables have been used in one global model [*Ming et al.*, 2007], the large dimensionality of the tables limits applicability of the model to computing systems with sufficient local memory to support the large tables.

To summarize the description of the activation schemes, Table 1 lists the treatments of mass transfer, the condensation coefficient, the integration over size distribution, the solution method, the treatment of kinetic limitations for each scheme. We do not have computational timings of every scheme, but we have found that the iterative Nenes, Shipway and Ming schemes are a factor of 20–100 times slower than the analytic ARG scheme, and that the timing of the ARG scheme can be reduced by a factor of 10 by replacing the error function in

the expression for activation (20) with the hyperbolic tangent approximation (23). The approximated ARG scheme is a factor of 200–1000 faster than the others. The timings of the Nenes and Shipway schemes are comparable, but the Ming scheme takes about three-fold more time than the Nenes and Shipway schemes because, in addition to iterating, it integrates numerically over the aerosol size distribution; consequently, in applications to a climate model [*Ming et al.*, 2007] it is replaced with a lookup table. The Nenes scheme requires about 30 iterations to converge, which explains the much larger timing compared with the ARG scheme.

3. Parameterization Performance

Our evaluation will focus on the *Abdul-Razzak and Ghan* [2000, hereinafter ARG], *Fountoukis and Nenes* [2005, hereinafter Nenes], *Ming et al.* [2006, hereinafter Ming], and *Shipway and Abel* [2010, hereinafter Shipway] parameterizations. Those are the physically-based schemes that are being or will be used in global models, and hence merit the greatest attention. For the Nenes scheme the *Barahona et al.* [2010] extension for condensation on inertia-limited particles is included.

In principle one could use atmospheric measurements of updraft velocity, droplet number concentration and aerosol composition and size distribution to evaluate models of the activation process. Although this has been done successfully [*Meskhidze et al.*, 2005; *Fountoukis et al.*, 2007], the conclusions are constrained by the limited parameter space explored and uncertainties of measuring updraft velocity and measuring both the aerosol below cloud and the droplet number within cloud. We therefore turn to detailed numerical solutions to provide benchmark simulations of cloud droplet nucleation.

To evaluate the performance of the parameterizations we compare results with numerical solutions for a variety of conditions. The numerical model we are using is that described by *Abdul-Razzak et al.* [1998], which is based on the general dynamic Köhler theory described by *Pruppacher and Klett* [1997], i.e., equations (4), (5), and (7). The aerosol size distribution is divided into 100 internally-mixed bins, with the bin boundaries spaced such that each bin has the same number of particles, and the central bin corresponding to the mean size of the distribution. For cases with multiple aerosol modes, 100 bins are devoted to each mode. The model produces results virtually identical to the numerical model of *Nenes et al.* [2001], which produced results in the middle of a range of results from different numerical models [*Kreidenweis et al.*, 2003]. However, it must be recognized that, as documented by *Kreidenweis et al.* [2003], inter-model differences in binning and the treatment of mass transfer of water vapor can lead to 30% differences in number nucleated. Indeed, the numerical model that the Ming scheme is based on produces results that differ significantly from those produced by this numerical model; those differences contribute to the differences between the

results from the Ming and other parameterizations. Although aerosol activation depends weakly on temperature and pressure, all simulations reported here are initialized at the same temperature (279 K) and pressure (1000 hPa). The initial relative humidity is assumed to be 90%, and the aerosol particles are assumed to be in thermodynamic equilibrium at that relative humidity. Simulations are run until maximum supersaturation is achieved, and the number activated is determined from the number of particles with wet sizes larger than their critical size for activation. Thus, particles whose critical supersaturation for activation is less than the maximum supersaturation but whose growth is too slow for them to reach their critical size by the time maximum supersaturation is reached are not considered activated [Nenes *et al.*, 2001]. This differs from the droplet definition of Nenes *et al.* [2001] who consider inertially-limited particles as droplets. Although this does not affect the numerical parcel simulations, Barahona *et al.* [2010] demonstrated that neglecting condensational depletion of water vapor on inertially-limited particles can lead to large overestimations in S_{max} and droplet number.

To explore the parameter space we first consider a baseline case and then evaluate the performance as selected parameters are varied from the baseline case. We first consider a baseline case with a single lognormal aerosol mode to establish the dependence of the performance on each of the parameters, and then address more general multimode cases that are more applicable to interpretation of the application to global models of aerosol effects on clouds. We have also compared the schemes using measured aerosol size distributions, but do not report those results here because they can be understood in terms of the multimode cases.

The first baseline case is a single lognormal mode with a total aerosol number concentration of 1000 cm^{-3} , a number mode radius of $0.05 \text{ }\mu\text{m}$, and a geometric standard deviation of 2. The aerosol is assumed to be composed of ammonium sulfate, which has a density of 1.71 g cm^{-2} and a hygroscopicity of 0.7. The condensation coefficient is assumed to be 1, and entrainment is neglected. The baseline updraft velocity is 0.5 m s^{-1} , which is typical of stratiform clouds that exhibit the greatest sensitivity to the aerosol.

Figure 3 shows the maximum supersaturation and number fraction activated as functions of updraft velocity. Although the parameterizations were designed for application to stratiform clouds, which usually have updraft velocities between 0.1 and 1 m s^{-1} [Meskhidze *et al.*, 2005], we show results for updrafts up to 10 m s^{-1} to demonstrate their applicability to cumulus clouds. The Nenes and Shipway schemes diagnose maximum supersaturation in good agreement with the numerical solution for all updraft velocities. The ARG scheme underestimates S_{max} for updrafts stronger than 1 m s^{-1} , while the Ming scheme overestimates maximum supersaturations for updrafts stronger than 2 m s^{-1} , which is beyond the updraft range

that it is used for. The Ming scheme underestimates S_{max} for updrafts weaker than 1 m s^{-1} , so it exaggerates the sensitivity to updraft velocity. Consistent with the performance for supersaturation, the Nenes and Shipway schemes diagnose the number fraction activated in excellent agreement with the numerical solution, except for updrafts weaker than 0.4 m s^{-1} , when the Nenes scheme underestimates activation by about 30%. The abrupt drop in number activated by the Nenes scheme for low updraft velocity arises when droplet activation is dominated by kinetic limitations and the expression used to derive S_{part} changes; this feature is evident in other figures as the parameter space is explored. Smoothing this transition out further will be the subject of a future study. The ARG scheme consistently underestimates the number activated by 10–20%. The Ming scheme underestimates activation by up to 40% for updrafts weaker than 1 m s^{-1} , but diagnoses activation quite accurately for strong updrafts.

Figure 4 explores the performance as a function of aerosol number concentration for a fixed updraft velocity of 0.5 m s^{-1} . The ARG scheme consistently underestimates S_{max} by about 10%, while the Nenes scheme diagnoses S_{max} remarkably well for aerosol number concentrations less than 1000 cm^{-3} , but underestimates S_{max} by about 20% for $N_a > 2000 \text{ cm}^{-3}$. Ming underestimates S_{max} by about 30% for $N_a > 2000 \text{ cm}^{-3}$ but overestimates S_{max} by up to 30% for low aerosol number concentrations. The Shipway scheme diagnoses S_{max} well for number concentrations less than 3000 cm^{-3} , but overestimates S_{max} for higher concentrations. Consequently, the ARG scheme consistently underestimates the number activated by about 10%, the Nenes scheme diagnoses the number activated remarkably well for $N_a < 1000 \text{ cm}^{-3}$ but underestimates activation by about 20% for $N_a > 2000 \text{ cm}^{-3}$, Ming underestimates activation for $N_a > 1000 \text{ cm}^{-3}$ by up to 50% but overestimates activation for $N_a < 300 \text{ cm}^{-3}$, and the Shipway scheme diagnoses the number activated well for $N_a < 3000 \text{ cm}^{-3}$ but overestimates activation by up to 100% as N_a approaches $10,000 \text{ cm}^{-3}$.

Figure 5 considers the dependence on the mode radius of the size distribution. As the distribution shifts to larger sizes more particles are activated earlier, limiting the supersaturation increase and resulting in smaller S_{max} . The ARG scheme diagnoses both S_{max} and the number activated remarkably well for all sizes. The Nenes and Shipway schemes both perform well for mode radius up to $0.1 \text{ }\mu\text{m}$, but for larger sizes they overestimate both S_{max} and the number activated significantly. The Ming scheme overestimates S_{max} and the number activated for mode radius less than $0.03 \text{ }\mu\text{m}$ or greater than $0.5 \text{ }\mu\text{m}$ and underestimates S_{max} and the number activated for intermediate mode radius. The surprisingly strong performance of the ARG scheme, which neglects kinetic limitations that one expects to be important at larger sizes, shows how empiricism (which the ARG scheme relies on more heavily than the other scheme) can

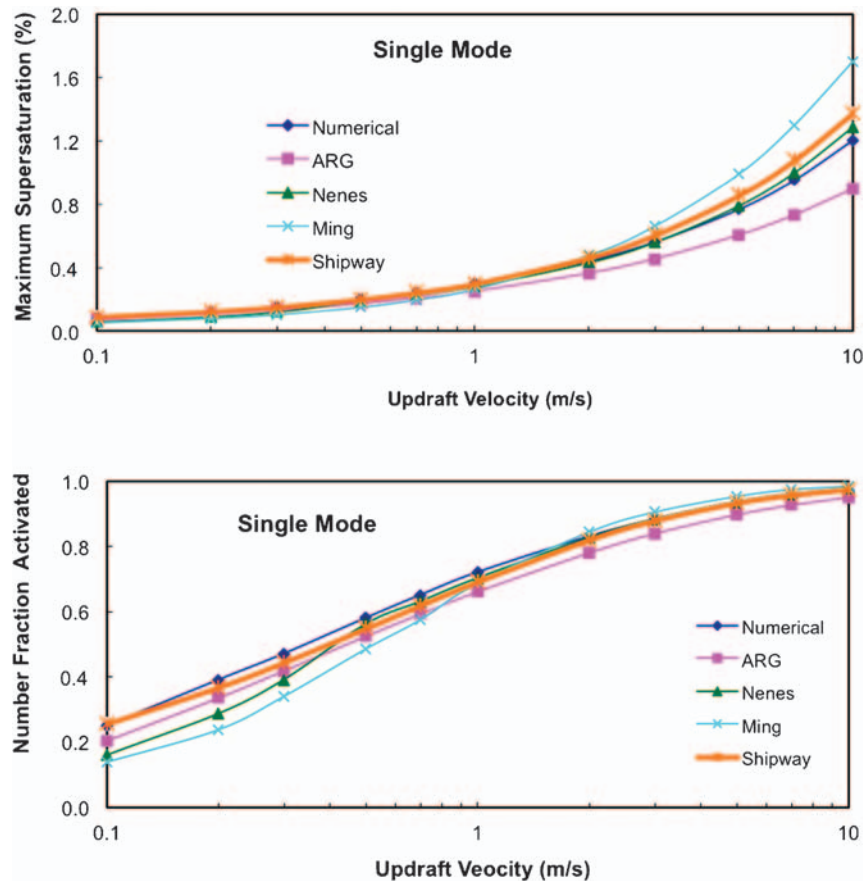


Figure 3. (top) Parameterized and simulated maximum supersaturation and (bottom) number fraction activated as functions of updraft velocity for a single lognormal aerosol mode with $N_a=1000 \text{ cm}^{-3}$, number mode radius = $0.05 \text{ }\mu\text{m}$, geometric standard deviation = 2, and composition of ammonium sulfate. ARG is the Abdul-Razzak and Ghan [2000] modal parameterization. Nenes is the Fountoukis and Nenes [2005] scheme. Ming is the Ming et al. [2006] scheme. Shipway is the Shipway and Abel [2010] scheme.

perform better for some conditions. However, as we shall see the ARG scheme does not perform as well under other conditions.

Figure 6 examines the performance as a function of the width of the aerosol size distribution. The numerical solution shows a decrease in S_{max} with increasing width because of the addition of larger particles that are activated earlier. The ARG and Ming schemes capture much of this dependence, although the Ming scheme underestimates S_{max} for all widths. The Nenes and Shipway schemes, on the other hand, produces almost no dependence on the width. Consequently, the ARG and Ming schemes correctly yield decreasing activation with increasing width, but the Nenes and Shipway schemes do not except for very narrow distributions.

The dependence of the performance on composition can be evaluated by considering the performance as a function of the hygroscopicity parameter κ , shown in Figure 7. The dependence is captured quite well by the ARG, Nenes and Shipway schemes. As in the cases of sensitivity to updraft velocity, aerosol number concentration, and mode radius, the Ming scheme exaggerates the

dependence of S_{max} on hygroscopicity. However, sensitivity of number activated to hygroscopicity is underestimated by the Ming scheme, because the number activated depends on both the maximum supersaturation and the sensitivity of activation to the supersaturation (which depends on hygroscopicity).

The activation process also depends on the value of the condensation coefficient, which has values reported between 0.01 and 1 [Mozurkewich, 1986]. Figure 8 examines the dependence of activation on the value. All four schemes capture this dependence quite well.

The dependence of maximum supersaturation and number activated on the entrainment rate is evaluated in Figure 9. The entrainment rate is expressed in terms of the ratio of the entrainment rate to the critical value e_c . The Barahona and Nenes [2007] treatment of the influence of entrainment has been applied to each of the parameterizations. All parameterizations capture this dependence accurately.

The influence of surfactants is illustrated in Figure 10, which evaluates the ARG and Nenes parameterizations as a

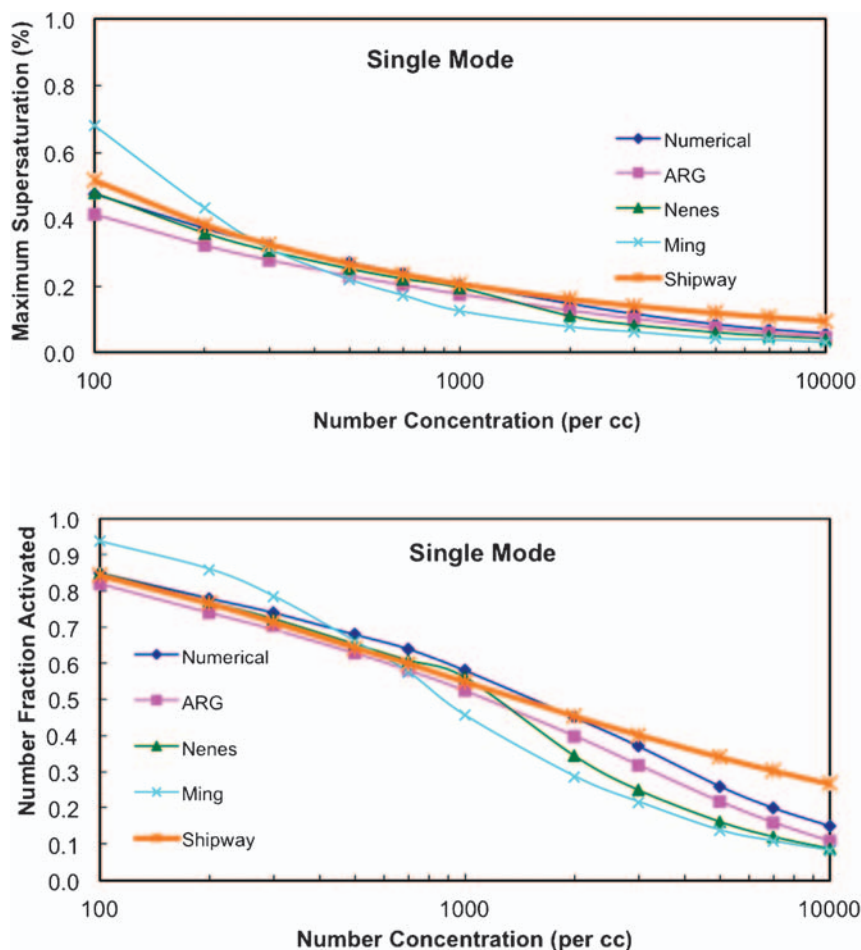


Figure 4. As in Figure 3, but as a function of aerosol number concentration for a fixed updraft velocity of 0.5 m s^{-1} . The baseline number concentration is 1000 cm^{-3} .

function of surfactant fraction of the aerosol. Both schemes correctly diagnose the increase in S_{max} and decrease in number activated with increasing surfactant fraction simulated by the numerical model. *Abdul-Razzak and Ghan [2004]* show that their treatment also performs well for the more realistic case of organic surfactants sampled in the Po Valley of Italy, which produces a very different dependence on organic surfactants.

A second class of cases to evaluate use a more general representation of the aerosol size distribution based on trimodal lognormal fits to measurements [*Whitby, 1978*]. Table 2 lists the lognormal parameters for several aerosol types.

Figure 11 evaluates the activation of the marine aerosol for updraft velocities between 0.1 and 10 m s^{-1} . The Nenes scheme diagnoses this more complex case remarkably well, but the ARG, Shipway and Ming schemes all produce biases. The Shipway scheme underestimates S_{max} by up to 30% and the ARG scheme underestimates the maximum supersaturation by 40% for all updraft velocities. Consequently, the Shipway and ARG schemes underestimate the activation of

the nuclei mode for strong updrafts and the accumulation mode for weak and moderate updrafts. Ming overestimates S_{max} for strong updrafts (beyond those it is used for) and hence overestimates activation of the nuclei mode for strong updrafts, but estimates the activation of the other modes quite well.

Figure 12 examines the performance for the clean continental aerosol. The Nenes and Shipway schemes both perform remarkably well, and the biases in the ARG scheme are smaller than for the marine aerosol. Ming performs well for the weaker updrafts it was designed for. For weaker updrafts the performance of the ARG and Ming schemes is comparable.

The activation of the Whitby background aerosol is evaluated in Figure 13. The ARG scheme underestimates S_{max} and activation of the accumulation mode by about 30% for all updraft velocities. The Nenes scheme performs very well for strong updrafts, but underestimates S_{max} and activation of the accumulation mode by about 30% for updrafts weaker than 0.6 m s^{-1} . The Ming scheme underestimates S_{max} and hence activation of the

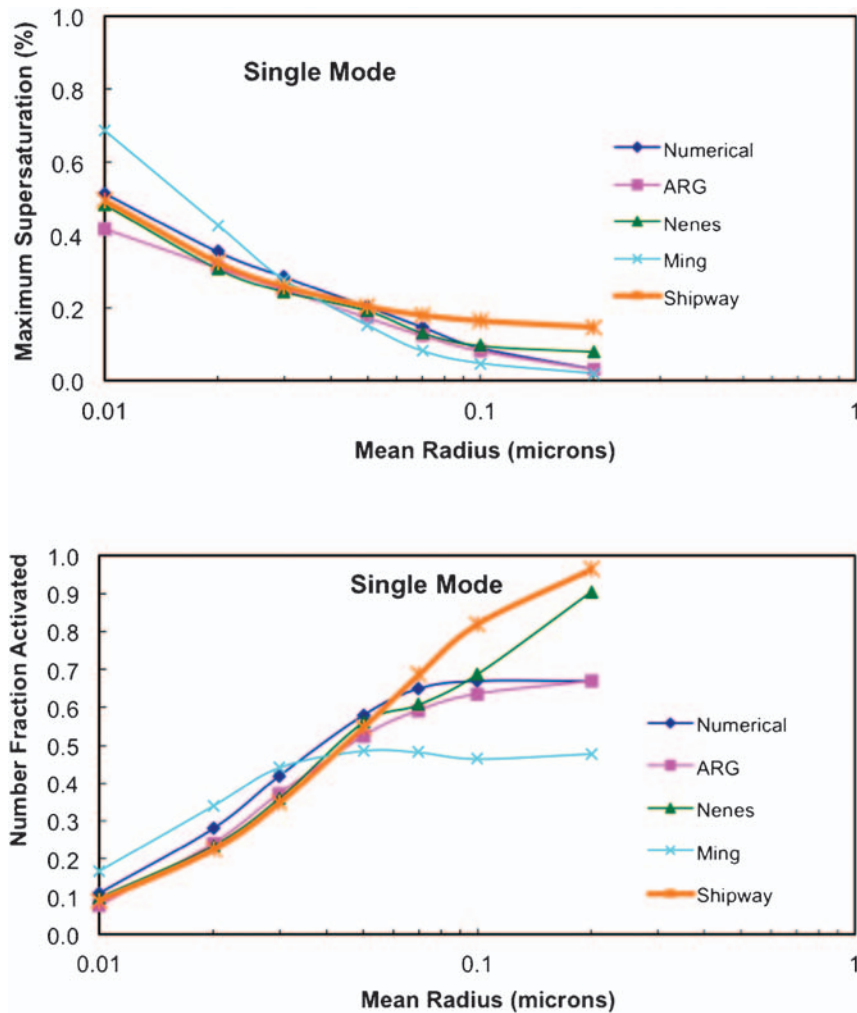


Figure 5. As in Figure 3, but as a function of number mode radius for a fixed updraft velocity of 0.5 m s^{-1} . The baseline number mode radius is $0.05 \text{ }\mu\text{m}$. Supersaturation does not reach a maximum in the numerical simulations for mode radius larger than $0.2 \text{ }\mu\text{m}$.

accumulation mode by up to 50% for updrafts weaker than 2 m s^{-1} . The Shipway scheme performs well for all updraft velocities.

For the Whitby urban aerosol (Figure 14), the Shipway scheme overestimates S_{max} and hence aerosol activation while the other schemes underestimate S_{max} and consequently aerosol activation. The Shipway scheme diagnoses S_{max} well for strong updrafts but for weak updrafts overestimates S_{max} by a factor of about two, and consequently overestimates activation for weak updrafts. The Nenes and Ming schemes diagnose S_{max} well for updrafts weaker than 0.5 m s^{-1} , but the ARG scheme is more accurate for updrafts stronger than 2 m s^{-1} . The Nenes, ARG and Ming schemes underestimate activation of the accumulation mode for strong updrafts, and the ARG scheme underestimates activation of the coarse mode for weak updrafts.

These results for the Whitby trimodal aerosol are consistent with those for the single mode aerosol. The Ming

scheme overestimates S_{max} and the number activated for low aerosol concentrations such as for the marine aerosol but underestimates S_{max} and activation for increasingly high aerosol concentrations such as the urban aerosol. The Shipway and Nenes schemes perform well under most conditions, except in polluted conditions when Shipway overestimates S_{max} . In some cases (dependence on width of distribution) the ARG scheme performs better than the Nenes and Shipway schemes because the former has been tuned to agree with the numerical simulations, but in other cases the Nenes and Shipway schemes perform better because they have more robust physics. The ARG scheme estimates lower S_{max} and activation than Nenes and Shipway for low aerosol concentrations and estimates more activation than Nenes for high aerosol concentrations, and hence is more sensitive to increases in aerosol concentration. Some of this difference is likely due to neglect of kinetic effects in the ARG scheme, which are more important for higher aerosol concentrations [Nenes *et al.*, 2001]. As we shall see,

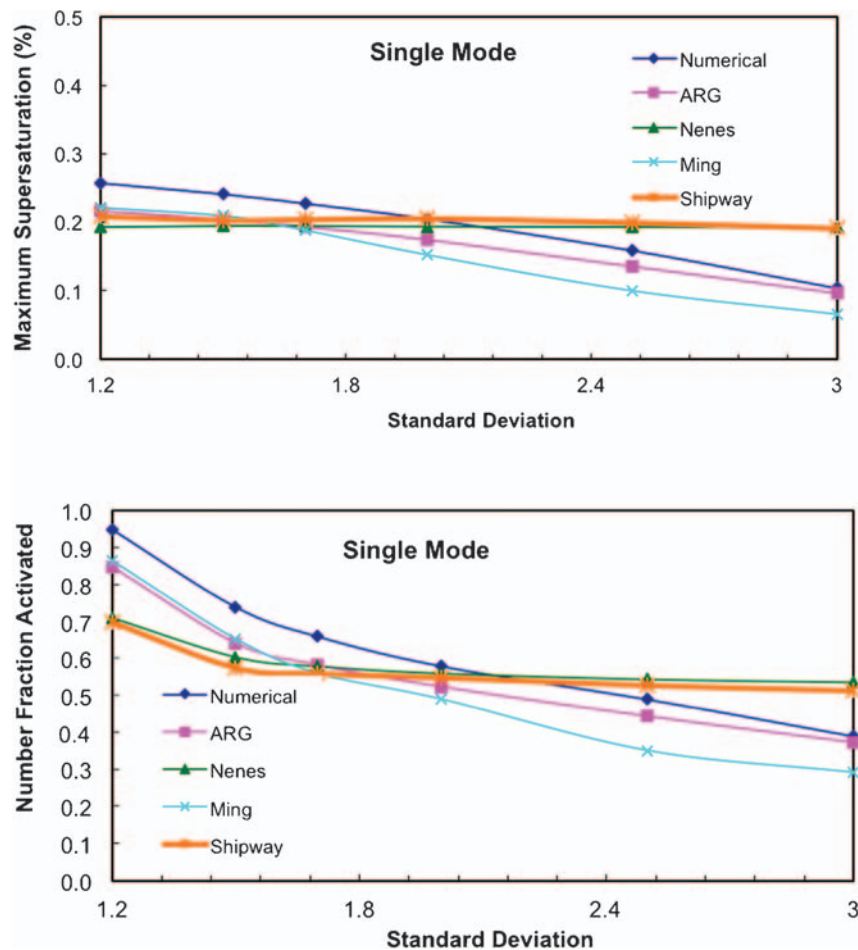


Figure 6. As in Figure 3, but as a function of geometric standard deviation of the lognormal size distribution, for a fixed updraft velocity of 0.5 m s^{-1} . The baseline geometric standard deviation is 2.

this has implications for effects of anthropogenic aerosol on clouds.

4. Applications

Physically-based droplet nucleation parameterizations have been applied to a variety of models. Applications are summarized in Table 3. In all applications the parameterizations are applied to double-moment models that predict droplet number concentration from the droplet number balance, in most models also including effects of collision/coalescence, collection and evaporation as well as nucleation [Ghan *et al.*, 1997]. The first applications were to global models because of interest in quantifying the aerosol indirect effect on climate. In such models a critical element of the application of droplet nucleation schemes is the representation of the updraft velocity, which as we have seen has a strong and nonlinear influence on droplet nucleation. Given the coarse resolution of global models, updrafts are not adequately resolved. Subgrid variations in updraft velocity and droplet nucleation must be represented. Ghan *et al.* [1997] show how this subgrid variability can be expressed in

terms of the subgrid probability distribution of updraft velocity, $p(w)$:

$$\bar{N}_n = \int_0^{\infty} N_{act}(w)p(w)dw \quad (47)$$

For turbulent boundary layers $p(w)$ can be approximated by a Gaussian distribution with mean given by the resolved vertical velocity and the standard deviation of the distribution, σ_w , related to the turbulence kinetic energy (e) by assuming the turbulence is isotropic: $\sigma_w^2 = \frac{2}{3}e$ [Lohmann *et al.*, 1999]. Alternatively, σ_w can be related to the eddy diffusivity (K): $\sigma_w = \frac{K}{l_c}$ [Morrison and Gettelman, 2008], where l_c is a prescribed mixing length. Since N_{act} is a complex function of updraft velocity the integral in (47) cannot be performed analytically. Some global models therefore integrate numerically [Ghan *et al.*, 2001a, 2001b; Ghan and Easter, 2006], but this can be computationally expensive. Most models [e.g., Lohmann *et al.*, 2007; Ming *et al.*, 2007; Gettelman *et al.*, 2008; Wang and Penner, 2009]

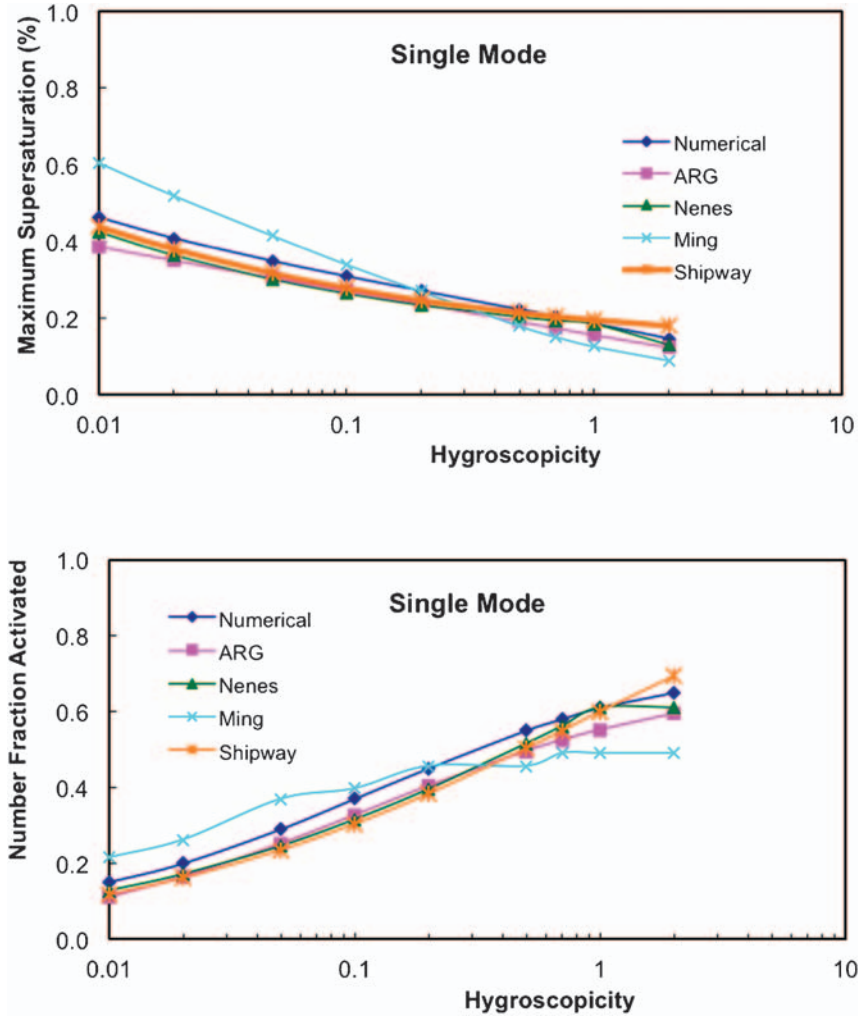


Figure 7. As in Figure 3, but as a function of hygroscopicity for a fixed updraft velocity of 0.5 m s^{-1} . The baseline hygroscopicity is 0.7.

therefore approximate the integral by evaluating N_{act} at only one updraft velocity, often the sum of the resolved updraft velocity and σ_w within the grid cell. *Morales and Nenes [2010]* have explored this issue more deeply, and have shown that for a Gaussian $p(w)$ use of a single characteristic updraft velocity given by $0.65\sigma_w$ yields grid cell mean droplet numbers within 10% of those with numerical integration over $p(w)$. In some models [*Ghan et al., 1997*] a minimum for σ_w is applied because the processes that drive turbulence are not represented well, and this minimum value is treated as a tuning parameter because it is not constrained well by measurements.

Since droplet nucleation is one of several terms in the droplet number balance, the estimate of the number nucleated must be converted to a droplet nucleation tendency. Several methods have been employed. *Ghan et al. [1997]* and *Ovtchinnikov and Ghan [2005]* distinguish between droplet nucleation in growing clouds and nucleation at the base of existing clouds:

$$\frac{dN_k}{dt} = \frac{df_k}{dt} \bar{N}_n + \frac{\min(f_k - f_{k-1}, 0)}{\Delta z} \int_{w_{min}}^{\infty} w N_{act}(w) dw \quad (48)$$

where f_k is the cloud fraction in layer k and w_{min} is a minimum updraft velocity estimated by assuming stronger updrafts occur in the cloudy fraction of the grid cell. Nucleation in the interior of existing clouds is neglected. The factor $f_k - f_{k-1}$ in (48) is the clear sky fraction below layer k , assuming maximum overlap.

A second method [*Lohmann et al., 1999*] to determine the tendency simply restores the droplet number toward the number nucleated:

$$\frac{dN}{dt} = \frac{\max(\bar{N}_n - N_c, 0)}{\Delta t} \quad (49)$$

where N_c is the droplet number and Δt is the time step. This treatment is applied to all layers where cloud is present. A

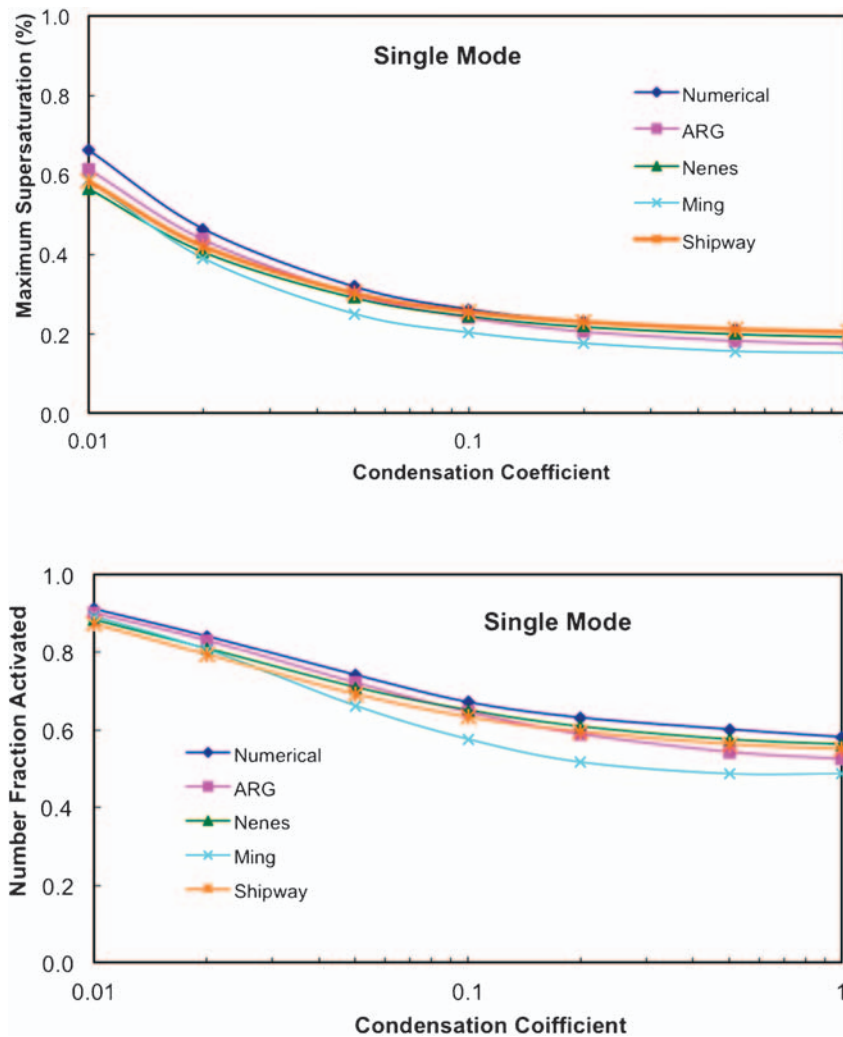


Figure 8. As in Figure 3, but as a function of the condensation coefficient for a fixed updraft velocity of 0.5 m s^{-1} . The baseline condensation coefficient is 1.

third method uses a prescribed activation timescale [Morrison and Gettelman, 2008] instead of the timestep in (49) to reduce the sensitivity to the timestep.

In most past applications the primary purpose of predicting droplet number has been to quantify the indirect effect of anthropogenic aerosol on the planetary energy balance through effects on droplet number, droplet effective radius, droplet collision/coalescence, cloud liquid water content, and cloud albedo [Chuang *et al.*, 1997; Lohmann *et al.*, 2000; Ghan *et al.*, 2001b; Chuang *et al.*, 2002; Takemura *et al.*, 2005; Chen and Penner, 2005; Ghan and Easter, 2006; Ming *et al.*, 2007; Storelmo *et al.*, 2006, 2008; Lohmann *et al.*, 2007; Seland *et al.*, 2008; Wang and Penner, 2009; Quaas *et al.*, 2009; Hoose *et al.*, 2009; Chen *et al.*, 2010a, 2010b; Salzmann *et al.*, 2010; Lohmann *et al.*, 2010; Lohmann and Ferrachat, 2010]. More recent applications have involved coupled atmosphere-ocean simulations to estimate effects on climate [Chen *et al.*, 2010b]. Many of the global models with these droplet number parameterizations are presently being used in climate

change simulations for the fifth assessment of climate change by the Intergovernmental Panel on Climate Change.

In the last few years, droplet nucleation parameterizations have also been applied to cloud-resolving models to provide a computationally efficient alternative to explicit prediction of supersaturation. This has led to several studies investigating aerosol effects on cumulus clouds [Lee *et al.*, 2008a, 2008b, 2009b, 2010], which have been neglected in most studies with global models. Other studies of such effects have been conducted using cloud models with size-resolved bin microphysics [Fridlind *et al.*, 2004; Khain *et al.*, 2004; Xue and Feingold, 2006; Fan *et al.*, 2007, 2009; Li *et al.*, 2008], which require explicit prediction of supersaturation and are much more computationally expensive, but offer the advantage of being able to treat droplet nucleation on the lateral edges and in the interior of the clouds.

Droplet nucleation parameterizations have also been applied to regional models that do not resolve cloud updrafts explicitly but provide a finer horizontal resolution

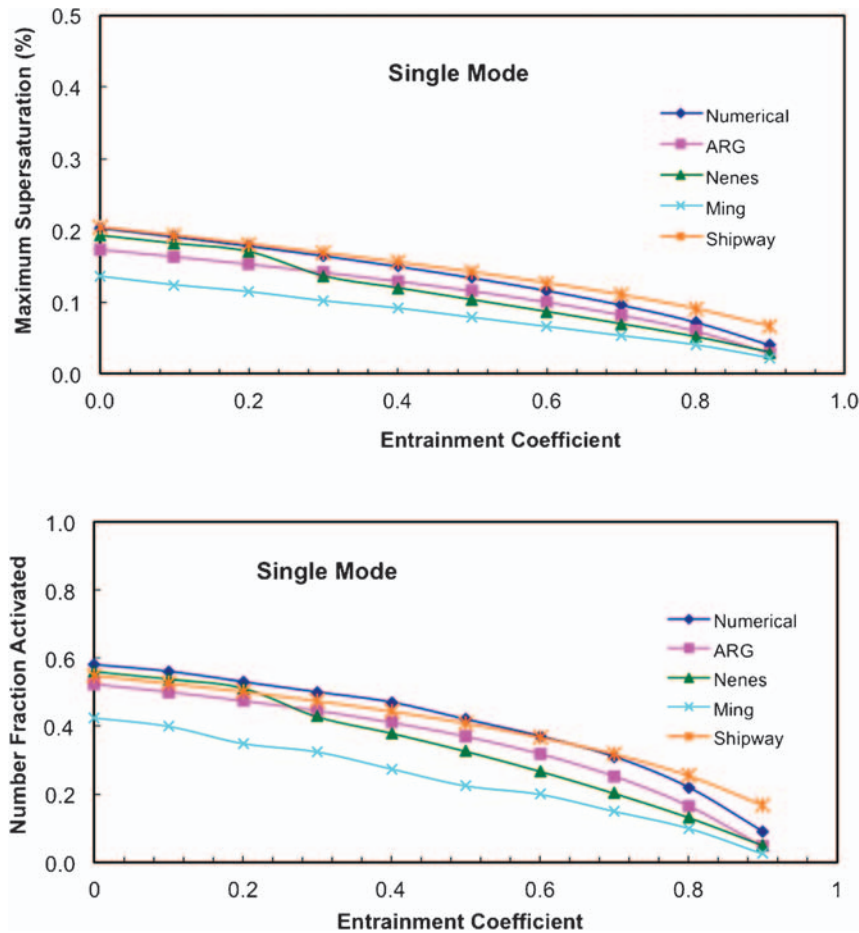


Figure 9. As in Figure 3, but as a function of entrainment rate for a fixed updraft velocity of 0.5 m s^{-1} . The baseline entrainment rate is 0.

than global models for a limited domain. Such models are well suited for evaluating simulated sensitivity of clouds to observed gradients in aerosol concentration [Gustafson *et al.*, 2007; Ivanova and Leighton, 2008; Bangert *et al.*, 2011].

Finally, one scheme has been applied recently to a multi-scale modeling framework [Wang *et al.*, 2011a], in which a cloud resolving model with double moment microphysics is applied to each grid cell of a global model. That model has been used to estimate global aerosol effects on cumulus as well as stratiform clouds [Wang *et al.*, 2011b].

5. Comparison of Parameterizations in a Global Model

The initial purpose of droplet nucleation parameterizations was to estimate aerosol effects on warm clouds. Although different parameterizations have been applied to a variety of models as summarized in Table 3, only recently have different parameterizations been applied to the same model so that their different influence on the estimated aerosol indirect effects can be unambiguously compared. The Abdul-Razzak and Ghan [2000] and Fountoukis and Nenes [2005] schemes have both been applied to the Community Atmosphere Model (CAM5), which has been released to the

public (<http://www.cesm.ucar.edu/models/cesm1.0/cam/>) with the ARG scheme only. A detailed description of CAM5 is available at http://www.cesm.ucar.edu/models/cesm1.0/cam/docs/description/cam5_desc.pdf.

Figure 15 compares the annual mean column droplet number simulated for present day emissions by CAM5 with the ARG and Nenes schemes. Although the same treatment of aerosol processes is used in each simulation, the aerosol distributions are slightly different (to within less than 10%, with no bias) because the droplet nucleation schemes produce slightly different simulations of nucleation scavenging of the aerosol. The simulated column droplet number concentrations are remarkably similar, with the Nenes scheme producing systematically larger concentrations by 0–20%. This result is consistent with the tendency of the Nenes scheme to diagnose higher activation fractions than the ARG scheme for most conditions, as demonstrated in Figures 3–14.

The comparison for preindustrial aerosol and precursor emissions (but with present day ocean surface temperatures and greenhouse gases), also shown in Figure 15, reveals a greater tendency of the Nenes scheme to produce larger droplet concentrations, by 20–50% compared with the ARG

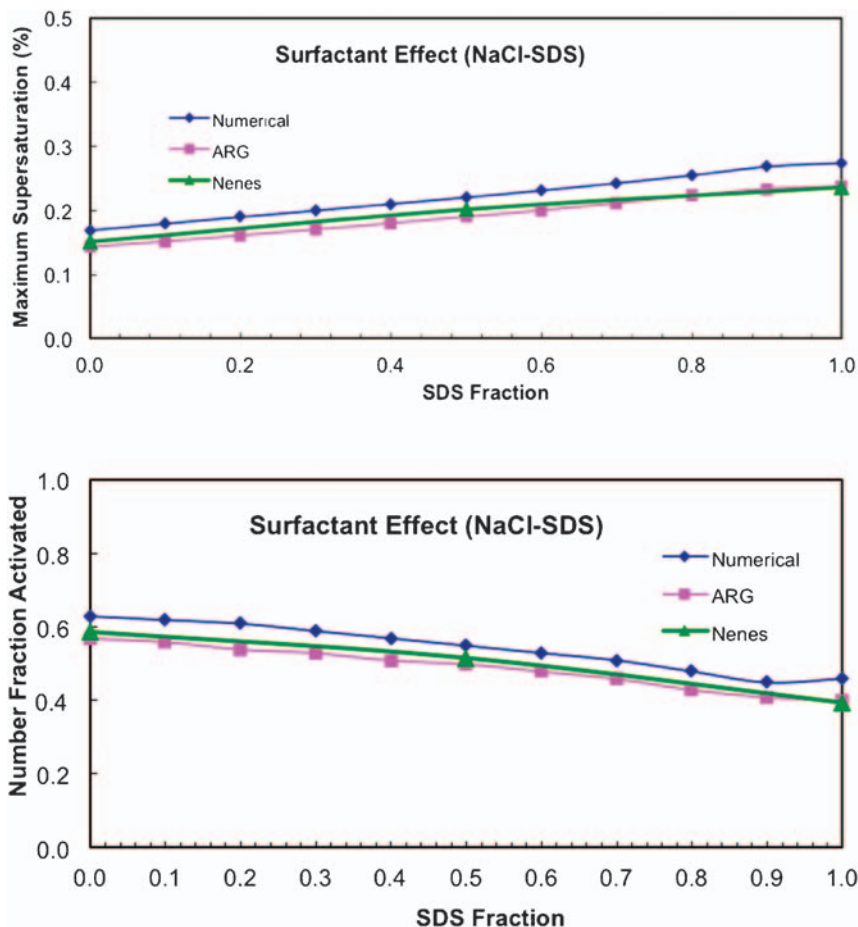


Figure 10. As in Figure 3, but as a function of surfactant mass fraction of the dry aerosol for a fixed updraft velocity of 0.5 m s^{-1} . The surfactant is sodium dodecyl sulfate and the salt is sodium chloride. The Ming and Shipway schemes do not account for the influence of surfactants.

scheme. This greater difference for preindustrial emissions (when aerosol number concentrations are lower) is not evident in Figure 4, which shows good agreement between the ARG and Nenes schemes for all number concentrations, but is apparent in comparing Figures 11–14, which clearly show greater differences in number activated for the Whitby marine aerosol and smaller differences for the increasingly polluted clean continental, background, and urban aerosol, the last indicating a reversal in the difference.

The greater difference in column droplet number concentrations from the two schemes for preindustrial conditions means smaller differences between present day and

preindustrial column droplet number concentrations for the Nenes scheme than for the ARG scheme, which translates into a smaller estimate for aerosol indirect effects: the global mean difference between present day and preindustrial shortwave cloud forcing (a measure of aerosol indirect effects because experiments neglecting absorption by black carbon produce similar results) is -1.60 W m^{-2} with the Nenes scheme but is -1.76 W m^{-2} for the ARG scheme. This is a much smaller difference than the two-fold differences between indirect effects estimated by completely different GCMs [Penner *et al.*, 2006; Forster *et al.*, 2007; Lohmann *et al.*, 2010], which suggests that differences in

Table 2. Aerosol Distribution Parameters (r_m in μm , N_m in cm^{-3})^a

	Nuclei Mode			Accumulation Mode			Coarse Mode		
	r_1	σ_1	N_1	r_2	σ_2	N_2	r_3	σ_3	N_3
Marine	0.005	1.6	340	0.035	2.0	60	0.31	2.7	3.1
Clean Continental	0.008	1.6	1000	0.034	2.1	800	0.46	2.2	0.72
Background	0.008	1.7	6400	0.038	2.0	2300	0.51	2.16	3.2
Urban	0.007	1.8	106000	0.027	2.16	32000	0.43	2.21	5.4

^aWhitby [1978].

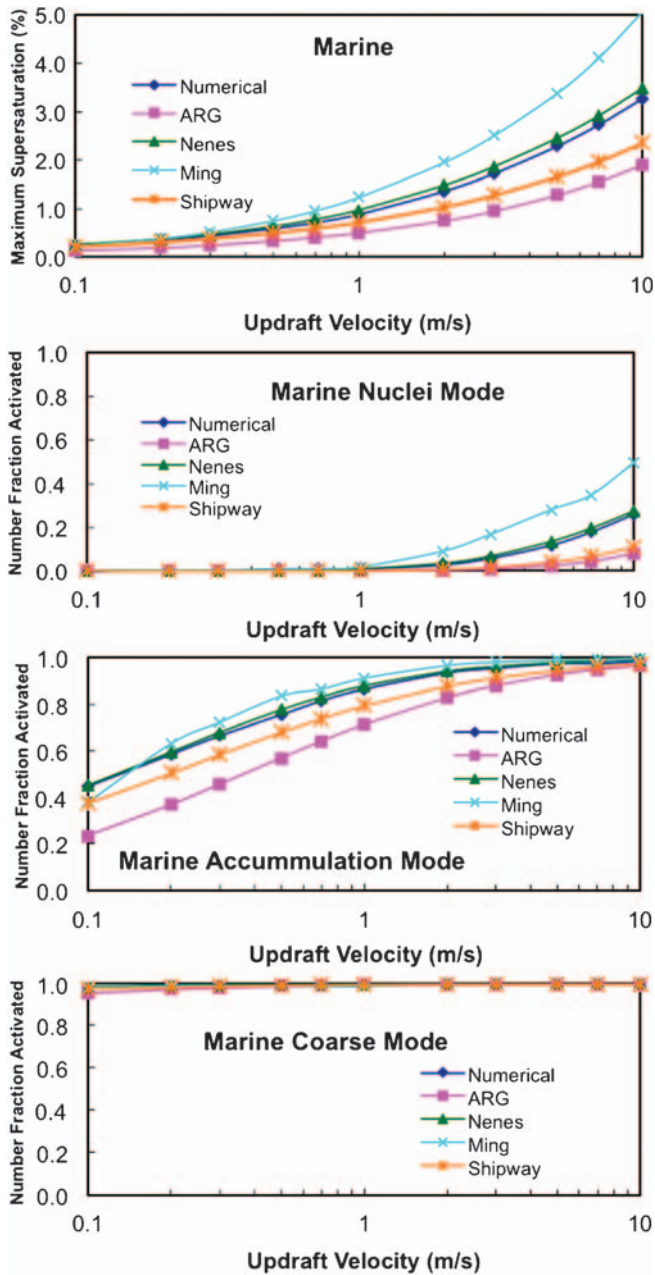


Figure 11. (top) Parameterized and simulated maximum supersaturation and (bottom) number fraction activated for each mode as functions of updraft velocity for the *Whitby* [1978] marine aerosol and composition of ammonium sulfate. Mode 1 is the nuclei mode. Mode 2 is the accumulation mode. Mode 3 is the coarse mode.

other aspects of the treatments of clouds and aerosol in GCMs are producing most of the differences between estimates of aerosol indirect effects.

Given the large difference in the timings of ARG and Nenes schemes discussed in section 2, the timing difference in a GCM is also of interest. In CAM5, the Nenes scheme almost doubles the total run time compared to simulations with the ARG scheme. The difference would be larger if

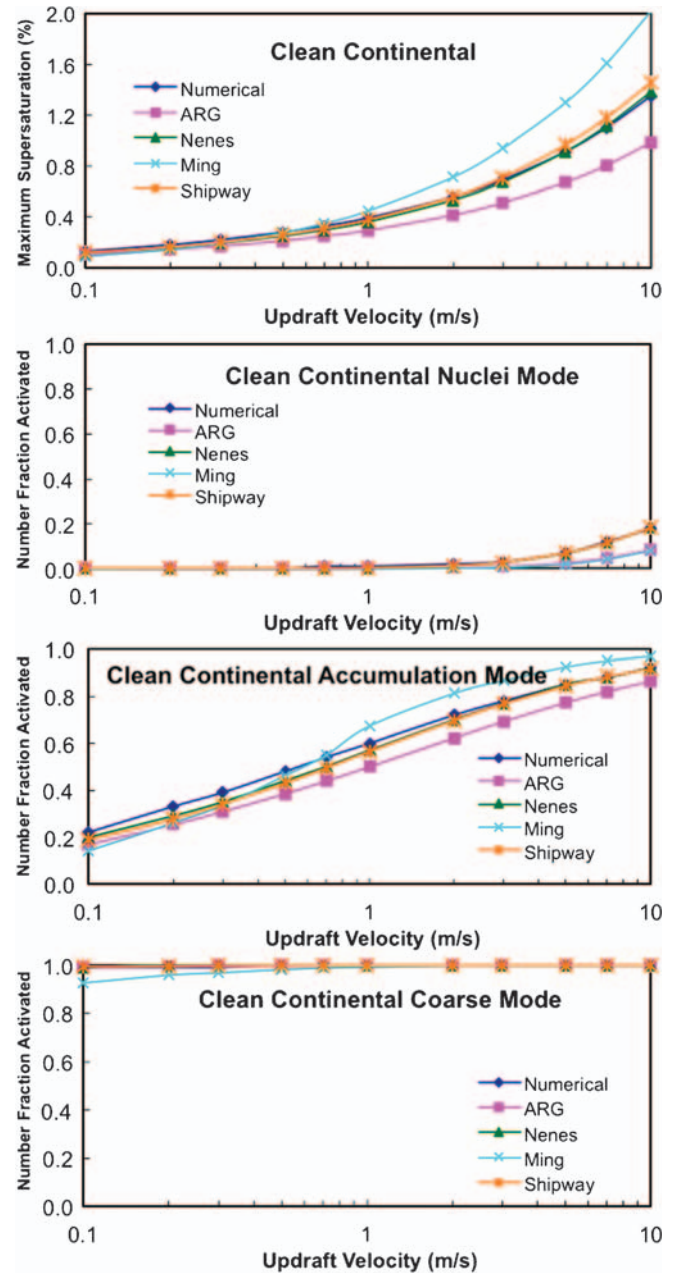


Figure 12. As in Figure 11, but for the *Whitby* [1978] clean continental aerosol.

droplet nucleation was calculated for multiple updraft velocities rather than a single updraft velocity, or for all cloudy layers rather than just at cloud base and in growing clouds. It would be smaller if the error function is replaced by the hyperbolic tangent approximation.

6. Further Development

Although the droplet nucleation schemes provide robust physically-based representations of aerosol effects on droplet nucleation, further development is needed in several directions.

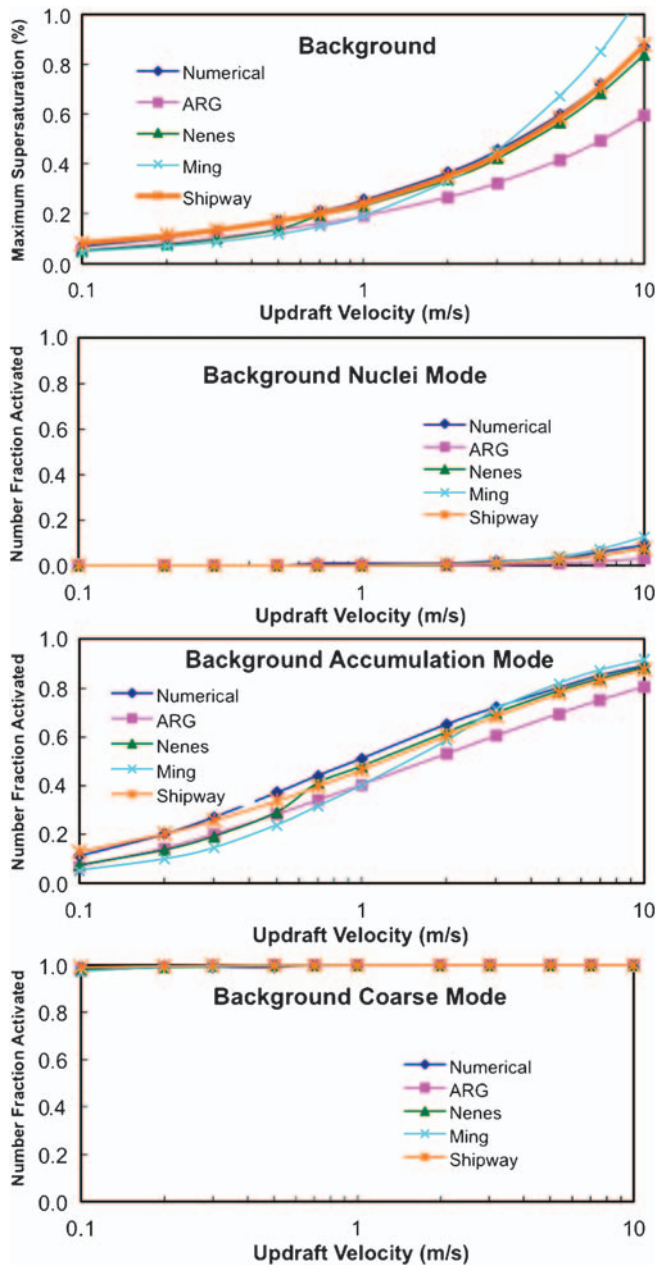


Figure 13. As in Figure 11, but for the *Whitby* [1978] background aerosol.

First, the influence of surfactants needs further development. Surfactant effects (that include bulk-surface partitioning of organics) should be applied to the lognormal Nenes scheme [Fountoukis and Nenes, 2005], and the influence needs to be connected to organic surfactants in application models. The influence of organics and particle phase state on droplet activation kinetics needs to be quantified and understood so that it can be represented in the parameterizations (e.g., parameterized as changes in the condensation coefficient). This issue remains an outstanding source of droplet number prediction uncertainty [Nenes et al., 2002]. Although secondary organic aerosol

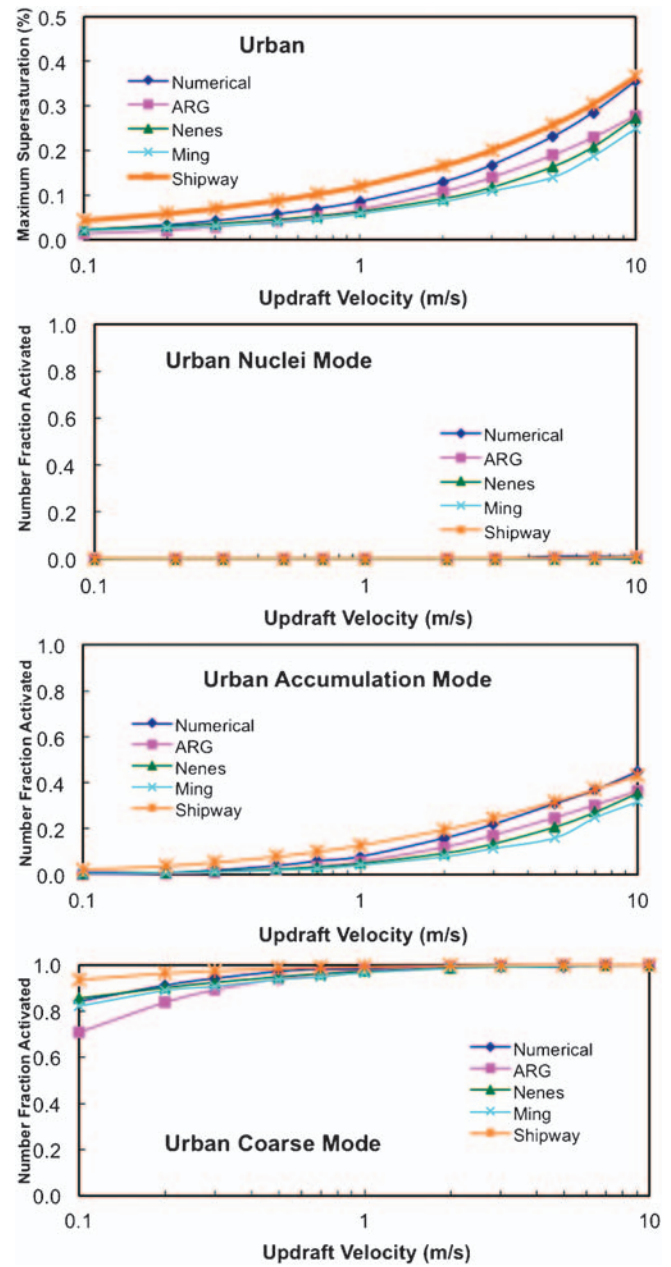


Figure 14. As in Figure 11, but for the *Whitby* [1978] urban aerosol.

and highly aged ambient aerosol with high organic content tends to exhibit rapid activation kinetics similar to CCN composed of pure NaCl and $(\text{NH}_4)_2\text{SO}_4$ [Engelhart et al., 2008; Moore et al., 2008; Bougiatioti et al., 2009; Murphy et al., 2009; Asa-Awuku et al., 2010; Padro et al., 2010; Engelhart et al., 2011], an emerging body of evidence suggests that secondary organic CCN of low hygroscopicity can exhibit substantially slower activation kinetics than CCN composed of pure NaCl or $(\text{NH}_4)_2\text{SO}_4$ [Chuang, 2003; Lance, 2007; Ruehl et al., 2008; Sorooshian et al., 2008; Asa-Awuku et al., 2009; Murphy et al., 2009; Ruehl et al., 2009; Shantz et al., 2010].

Table 3. Models That Physically-Based Droplet Nucleation Parameterizations Have Been Applied to

Model Name	Type	Parameterization	Reference
CCM1	global	Abdul-Razzak	<i>Ghan et al. [1997]</i>
ECHAM	global	Chuang et al.	<i>Chuang et al. [1997, 2002]</i>
ECHAM5-HAM	global	Chuang et al.	<i>Lohmann et al. [1999]</i>
MIRAGE	global	Hänel	<i>Lohmann et al. [2000]</i>
CAM3	global	Lin and Leach	<i>Roelofs et al. [2006]</i>
CAM3-Oslo	global	Abdul-Razzak	<i>Lohmann et al. [2007]</i>
CAM3-UMich	global	Abdul-Razzak	<i>Ghan et al. [2001a, 2001b]</i>
CAM3.5-PNNL	global	Abdul-Razzak	<i>Ghan and Easter [2006]</i>
CAM3.5	global	Abdul-Razzak	<i>Gettelman et al. [2008]</i>
CAM5	global	Abdul-Razzak	<i>Storelvmo et al. [2006, 2008]</i>
CAM5	global	Nenes	<i>Lee et al. [2009a]</i>
CAM5	global	Nenes	<i>Quaas et al. [2009]</i>
CAM5	global	Nenes	<i>Song and Zhang [2011]</i>
CAM5	global	Nenes	This study.
CAM5	global	Nenes	This study.
CAM5	global	Nenes	Meskhidze et al. (submitted to <i>Atmospheric Chemistry and Physics</i> , 2011)
IMPACT-CAM	global	Abdul-Razzak	<i>Wang and Penner [2009]</i>
GISS MATRIX	global	Abdul-Razzak	<i>Bauer et al. [2008]</i>
GISS-TOMAS	global	Nenes	<i>Sotiropoulou et al. [2007]</i>
		Nenes	<i>Hsieh [2009]</i>
		Nenes	<i>Chen et al. [2010a, 2010b]</i>
		Nenes	Leibensperger et al. (manuscript in preparation, 2011)
		Nenes	Lee et al. (manuscript in preparation, 2011)s
		Nenes	<i>Westervelt et al. [2011]</i>
NASA GMI	global	Nenes	<i>Barahona et al. [2011]</i>
		Nenes	Karydis et al. (submitted to <i>Journal of Geophysical Research</i> , 2011)
		Nenes	Sotiropoulou et al. (manuscript in preparation, 2011)
SPRINTARS	global	Abdul-Razzak	<i>Takemura et al. [2005]</i>
ECHAM	global	Abdul-Razzak	Stier (manuscript in preparation, 2011)
GAMIL	global	Abdul-Razzak	<i>Shi [2010]</i>
		Nenes	<i>Shi [2010]</i>
HadGEM-UKCA	global	Abdul-Razzak	West et al. (manuscript in preparation, 2011)
GLOMAP	global	Nenes	<i>Pringle et al. [2009]</i>
GEOS5	global	Nenes	<i>Sud et al. [2009]</i>
AM2	Global	Ming	<i>Ming et al. [2007]</i>
AM3	global	Ming	<i>Salzmann et al. [2010]</i>
AM3	single column	Ming	<i>Guo et al. [2010]</i>
MM5	regional	Abdul-Razzak	<i>Morrison et al. [2008]</i>
WRF	regional	Abdul-Razzak	<i>Gustafson et al. [2007]</i>
MC2	regional	Abdul-Razzak	<i>Ivanova and Leighton [2008]</i>
COSMO-ART	regional	Abdul-Razzak	<i>Bangert et al. [2011]</i>
ICLAMS	regional	Nenes	<i>Solomos et al. [2011]</i>
ATHAM	cloud-resolving	Abdul-Razzak	<i>Guo et al. [2007]</i>
GCE	cloud-resolving	Abdul-Razzak	<i>Lee et al. [2009a]</i>
NASA Langley CRM	cloud-resolving	Abdul-Razzak	<i>Luo et al. [2008]</i>
WRF	cloud-resolving	Ming	<i>Lee et al. [2008a, 2008b]</i>
SAM	cloud-resolving	Abdul-Razzak	unpublished
UK Met Office LEM	cloud-resolving	Shipway	unpublished
MACM	multiscale	Abdul-Razzak	<i>Wang et al. [2011a, 2011b]</i>

Second, the hygroscopicity of insoluble particles (such as dust and volcanic ash) can originate from the presence of soluble salts in the particles, and, from the adsorption of water vapor on their surface. The relative importance of each, together with the dry particle size, controls their critical supersaturation [*Kumar et al., 2009a, 2011a; Latham et al., 2011*]. The combined effect of adsorption and solute can be comprehensively accounted for by implementing the unified activation theory of *Kumar et al. [2011b]* within the activation parameterizations presented here [e.g., *Kumar et al., 2009b*].

Third, although field measurements have been used to evaluate the Köhler theory and one of the parameterizations described here [*Meskhidze et al., 2005; Fountoukis et al., 2007*], information about the particle composition in those evaluations has been limited. Further evaluation is needed using particle size and composition information now available from single-particle mass spectrometers mounted behind a counterflow virtual impactor that samples and evaporates cloud droplets, leaving behind the particle upon which the droplet formed.

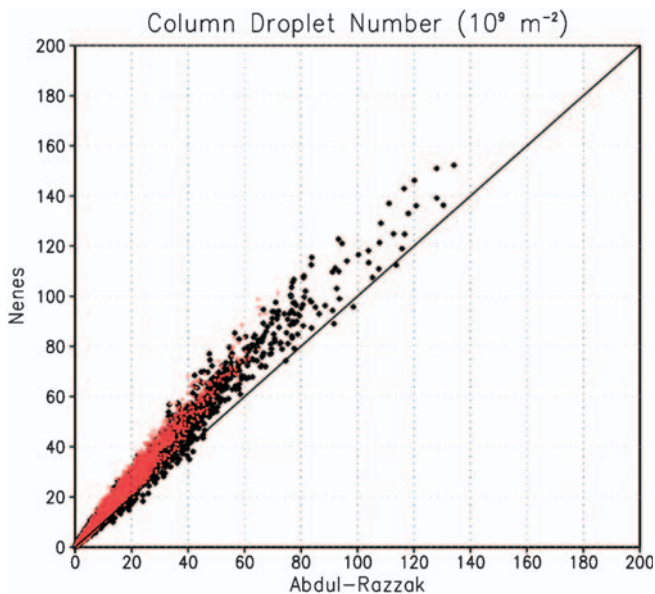


Figure 15. Gridpoint comparison of the annual mean column droplet number concentration simulated by CAM5 for present day (black) and preindustrial (red) emissions with the Abdul-Razzak and Nenes schemes. Each simulation was run for five years.

Fourth, the schemes need to be applied to shallow cumulus clouds, including the effects of entrainment [Barahona and Nenes, 2007; Barahona et al., 2011]. This should be straightforward for models with shallow cumulus schemes that diagnose mass flux and cloud fraction and hence updraft velocity [Bretherton and Park, 2009; Park and Bretherton, 2009]. Evaluation of the entrainment effect formulation [Barahona and Nenes, 2007] by Morales et al. (manuscript in preparation, 2011) for shallow and moderate-size cumulus suggests that it substantially improves the prediction of droplet number (compared to using an adiabatic formulation).

Fifth, the schemes also should be applied to deep cumulus parameterizations. Although the representation of cloud microphysics in deep cumulus parameterizations has been crude for many years, recent developments [Lohmann, 2008; Song and Zhang, 2011] suggest it is time to apply double-moment microphysics schemes to cumulus parameterizations. Menon and Rotstayn [2006] applied an empirical relationship between aerosol and droplet number to cumulus clouds in a global model, and Lohmann [2008] applied a variation on the Ghan et al. [2003] scheme to deep cumulus clouds. Although application of physically-based nucleation schemes to droplet formation at the base of cumulus clouds is straightforward in cumulus parameterizations that diagnose updraft velocity, secondary nucleation of droplets can also be important for deep cumulus clouds [Pinsky and Khain, 2002; Segal et al., 2003; Heymsfield et al., 2009]. Secondary nucleation occurs above the base of deep cumulus clouds when updrafts are so strong that the supersaturation production

term in equation (5) drives supersaturation even in the presence of large liquid water contents. To see this, we note that in strong updrafts in the cloud interior the droplets are not in thermodynamic equilibrium ($S \gg S_{eq}$), so that the expression for the condensation rate can be simplified to

$$\frac{dW}{dt} = \frac{4\pi S \rho_w}{\rho_a V} \sum_i r_i G. \quad (50)$$

Then, assuming the Lagrangian supersaturation tendency $\frac{dS}{dt}$ is small compared to supersaturation production in updrafts and supersaturation depletion by condensation, the supersaturation balance can be approximated [Korolev, 1995; Morrison et al., 2005; Ming et al., 2007] by applying (50) to (5):

$$\alpha_w = \gamma^* G S N \bar{r} \quad (51)$$

where the dependence of G on hydrometeor size is neglected and the summation over hydrometeors in (50) has been expressed in terms of the number of hydrometeors and their mean radius \bar{r} . Equation (50) can be directly solved for the supersaturation. The potential utility of this diagnostic method was explored by Dearden [2009] in a kinematic framework that neglects the reduction in droplet number due to collision/coalescence and precipitation. To consider the influence of these effects we have applied (49) to the updrafts and cloud microphysics simulated by a cloud-resolving model with explicit cloud microphysics. The results are illustrated in Figures 16 and 17, where the diagnosed supersaturation is compared with that predicted in a model simulation of convective clouds forming near Kwajalein Island during the Kwajalein Experiment, KWAJEX [Yuter et al., 2005]. In this example, a cloud-resolving model [Khairoutdinov and Randall, 2003] with spectral bin cloud microphysics [Khain et al., 2004] is run in a two-dimensional configuration using 320 columns and 144 levels, with uniform 100-m horizontal and vertical resolution below 10 km and a stretched vertical grid above. Boundary conditions and prescribed large-scale forcing are from Blossey et al. [2007] and the fields presented here are for 0930 UTC 17 August 1999. Although hydrometeor radius in the strong updrafts is generally much greater than droplet radius near cloud base, the number of hydrometeors is greatly depleted by collision and coalescence and precipitation fallout, so that the product of number and radius may be smaller in the updrafts than where primary nucleation occurs near cloud base. For the case of precipitating convective clouds shown here, both methods determine supersaturations up to 5%, which are high enough to activate much of the interstitial aerosol in the interior of the cloud. Although the diagnostic method does not explain all of the variations in simulated supersaturation because it neglects other terms in the supersaturation budget (such as the Lagrangian tendency, which is important near cloud base), it estimates supersaturation to within 30% at most points, which suggests it is certainly better than

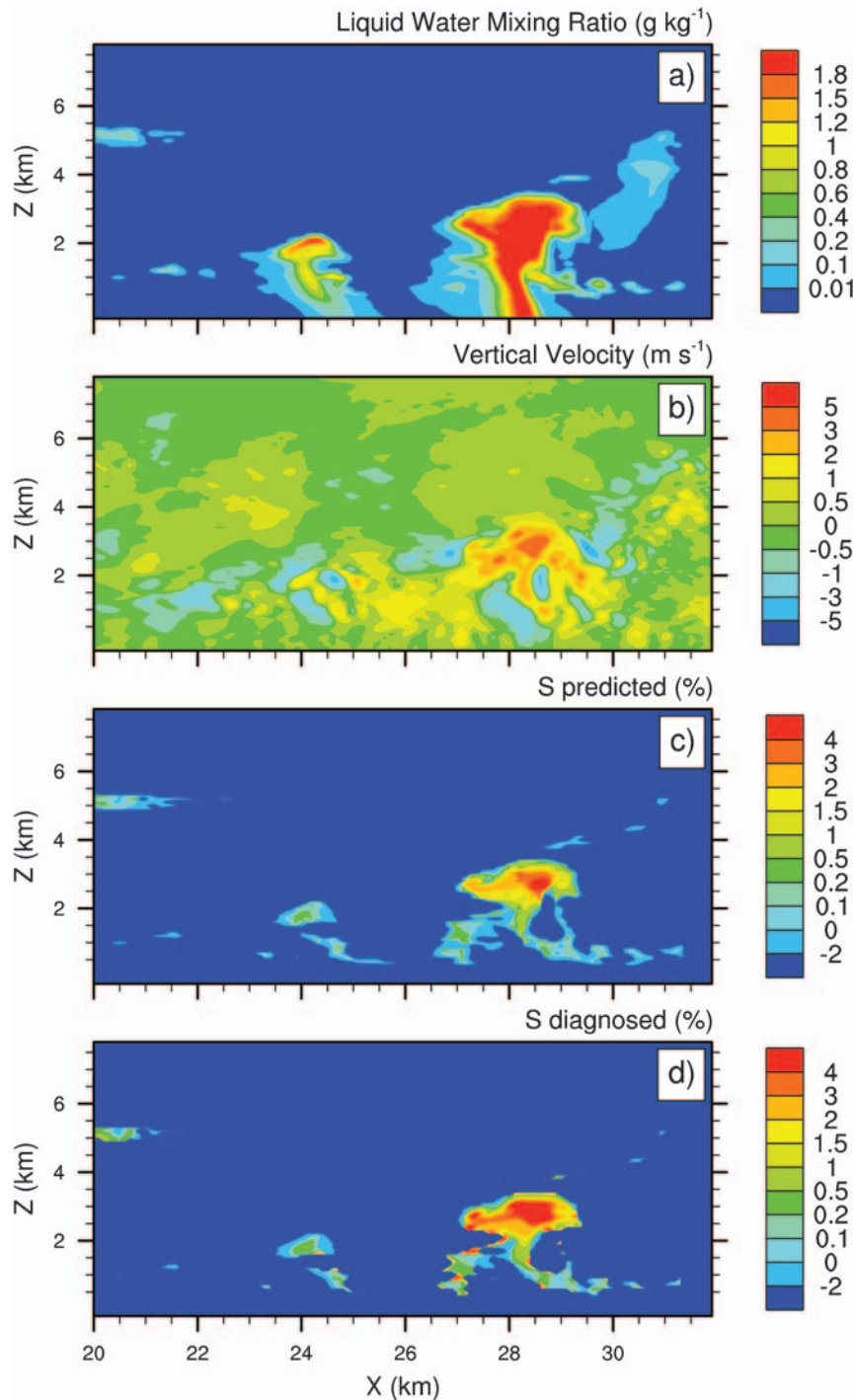


Figure 16. Vertical cross-sections of (a) liquid water mixing ratio, (b) vertical velocity and (c) supersaturation simulated by the SAM_SBM, and (d) diagnosed supersaturation derived from the supersaturation balance equation (49) using simulated updrafts and parameters of hydrometeor distributions. Only part of the model domain is shown to enhance details.

neglecting supersaturation in deep cumulus clouds. However, further analysis under a wider variety of conditions is needed to determine whether extensions to this simple model are needed.

Finally, observational and modeling analysis [Korolev and Mazin, 1993; Korolev, 1994, 1995; Magaritz et al., 2009]

suggests secondary nucleation also occurs in the interior of stratiform clouds when drizzle or evaporation depletes droplet surface area and the updraft velocity exceeds a threshold given by (49) such that the supersaturation exceeds the critical supersaturation of the most easily activated interstitial particles. Although analysis of trajectories by the cited

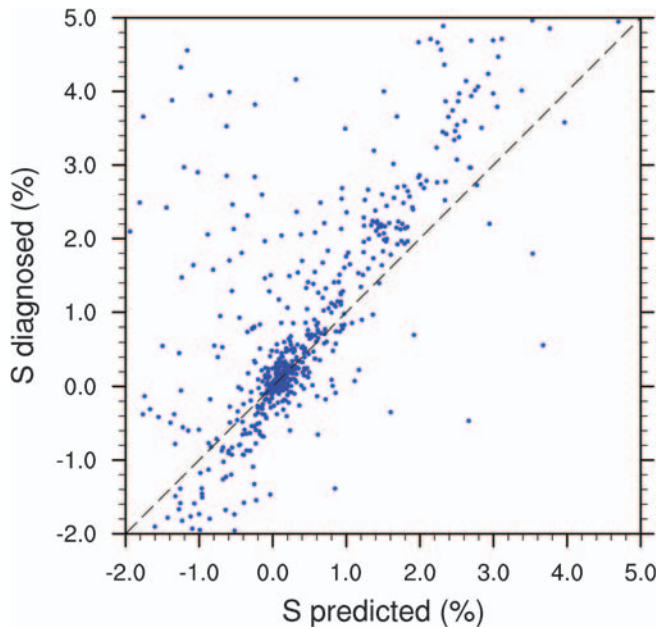


Figure 17. Point-by-point comparison of supersaturation diagnosed from the supersaturation balance equation (49), using simulated updrafts and parameters of hydrometeor distributions, with the supersaturation explicitly simulated by the cloud model's microphysics scheme.

authors suggests secondary nucleation occurs frequently in rising air parcels that had previously descended and lost droplets to evaporation, it is not clear whether a net increase in droplet number due to secondary nucleation is sufficiently common in stratiform clouds that it needs to be represented in cloud models.

7. Conclusions

The state of the art of representing aerosol effects on droplet nucleation in models has advanced considerably in the last two decades. Several physically-based methods produce estimates of maximum supersaturation and the number concentrations of droplets nucleated in good agreement (to within 30%) with detailed numerical integrations of the nucleation process under a wide variety of conditions. However, consistent differences are found for all schemes, and larger differences are found for the Ming scheme. The ARG scheme estimates lower S_{max} and activation than Nenes for low aerosol concentrations and estimates more activation than Nenes for high aerosol concentrations, and hence is more sensitive to increases in aerosol concentration. The Shipway scheme agrees with the Nenes scheme except under polluted conditions, when the Shipway scheme overestimates supersaturation and activation. The Ming scheme overestimates S_{max} and the number activated for low aerosol concentrations such as for the marine aerosol but underestimates S_{max} and activation for increasingly high aerosol concentrations such as the urban aerosol. These differences

are attributed to differences between the detailed numerical models that were used to develop the schemes. In particular, the ARG scheme was tuned using simulations by the same numerical model used in this comparison, while the kinetic effects in the Ming scheme were empirically determined using simulations by a numerical model that agrees much better with the Ming parameterization than with the numerical simulations reported here. This suggests the need to compare simulations by numerical models to determine the conditions in which the simulations of droplet nucleation agree and disagree, and to determine which models need revision to reduce differences between the simulations. Kreidenweis *et al.* [2003] explore this issue to some extent, but a more complete investigation that separates numerics from physics and chemistry is clearly needed.

Two of the nucleation parameterizations have been applied to the same global model. The 10% difference in droplet number produced by the two schemes can be explained on the basis of the offline tests presented here. Because the second indirect effect amplifies the first indirect effect (which scales as the cube root of droplet number and hence would produce only a 3% difference), the 10% droplet number difference produces a 10% difference (0.2 W m^{-2}) in the estimated effect of anthropogenic aerosol on short-wave cloud forcing (a measure of the aerosol first and second indirect effect).

Further extensions of this work include applications to treat the global influence of organic surfactants on clouds and the influence of aerosol on shallow and deep cumulus clouds. Thus, although in some respects the work on this subject is mature, there are plenty of opportunities to improve on the progress reported here.

Acknowledgments: This summary of the state of science has been funded by the U.S. Department of Energy Atmospheric Systems Research program. This manuscript has been authored by Battelle Memorial Institute, Pacific Northwest Division, under contract DE-AC05-76RL01830 with the US Department of Energy. AN acknowledges support by NASA ACPMAP and NSF CAREER.

References

- Abdul-Razzak, H., and S. J. Ghan 2000, A parameterization of aerosol activation 2. Multiple aerosol types, *J. Geophys. Res.*, **105**(D5), 6837–6844, doi: [10.1029/1999JD901161](https://doi.org/10.1029/1999JD901161).
- Abdul-Razzak, H., and S. J. Ghan 2002, A parameterization of aerosol activation 3. Sectional representation, *J. Geophys. Res.*, **107**(D3), 4026., doi: [10.1029/2001JD000483](https://doi.org/10.1029/2001JD000483).
- Abdul-Razzak, H., and S. J. Ghan 2004, Parameterization of the influence of organic surfactants on aerosol activation, *J. Geophys. Res.*, **109**, D03205. doi: [10.1029/2003JD004043](https://doi.org/10.1029/2003JD004043).
- Abdul-Razzak, H., S. J. Ghan, and C. Rivera-Carpio 1998, A parameterization of aerosol activation - 1. Single aerosol

- type, *J. Geophys. Res.*, **103**(D6), 6123–6131, doi: [10.1029/97JD03735](https://doi.org/10.1029/97JD03735).
- Albrecht, B. A. 1989, Aerosols, cloud microphysics, and fractional cloudiness, *Science*, **245**(4923), 1227–1230, doi: [10.1126/science.245.4923.1227](https://doi.org/10.1126/science.245.4923.1227).
- Andrejczuk, M., J. M. Reisner, B. Henson, M. K. Dubey, and C. A. Jeffery 2008, The potential impacts of pollution on a nondrizzling stratus deck: Does aerosol number matter more than type? *J. Geophys. Res.*, **113**(D19), doi: [10.1029/2007JD009445](https://doi.org/10.1029/2007JD009445).
- Andrejczuk, M., W. W. Grabowski, J. Reisner, and A. Gadian 2010, Cloud-aerosol interactions for boundary layer stratocumulus in the Lagrangian cloud model, *J. Geophys. Res.*, **115**, D22214, doi: [doi:10.1029/2010JD014248](https://doi.org/10.1029/2010JD014248).
- Asa-Awuku, A., G. J. Engelhart, B. H. Lee, S. N. Pandis, and A. Nenes 2009, Relating CCN activity, volatility, and droplet growth kinetics of beta-caryophyllene secondary organic aerosol, *Atmos. Chem. Phys.*, **9**(3), 795–812, doi: [10.5194/acp-9-795-2009](https://doi.org/10.5194/acp-9-795-2009).
- Asa-Awuku, A., A. Nenes, S. Gao, R. C. Flagan, and J. H. Seinfeld 2010, Water-soluble SOA from Alkene ozonolysis: Composition and droplet activation kinetics inferences from analysis of CCN activity, *Atmos. Chem. Phys.*, **10**(4), 1585–1597, doi: [10.5194/acp-10-1585-2010](https://doi.org/10.5194/acp-10-1585-2010).
- Bangert, M., C. Kottmeier, B. Vogel, and H. Vogel 2011, Regional scale effects of the aerosol cloud interaction simulated with an online coupled comprehensive chemistry model, *Atmos. Chem. Phys. Discuss.*, **11**(1), 1–37, doi: [10.5194/acpd-11-1-2011](https://doi.org/10.5194/acpd-11-1-2011).
- Barahona, D., and A. Nenes 2007, Parameterization of cloud droplet formation in large-scale models: Including effects of entrainment, *J. Geophys. Res.*, **112**, D16206, doi: [10.1029/2007JD008473](https://doi.org/10.1029/2007JD008473).
- Barahona, D., R. E. L. West, P. Stier, S. Romakkaniemi, H. Kokkola, and A. Nenes 2010, Comprehensively accounting for the effect of giant CCN in cloud activation parameterizations, *Atmos. Chem. Phys.*, **10**(5), 2467–2473, doi: [10.5194/acp-10-2467-2010](https://doi.org/10.5194/acp-10-2467-2010).
- Barahona, D., R. Sotiropoulou, and A. Nenes 2011, Global distribution of cloud droplet number concentration, autoconversion rate and aerosol indirect effect under diabatic droplet activation, *J. Geophys. Res.*, **116**, D09203, doi: [10.1029/2010JD015274](https://doi.org/10.1029/2010JD015274).
- Bauer, S. E., D. L. Wright, D. Koch, E. R. Lewis, R. McGraw, L. S. Chang, S. E. Schwartz, and R. Ruedy 2008, MATRIX (Multiconfiguration Aerosol TRacker of mIXing state): An aerosol microphysical module for global atmospheric models, *Atmos. Chem. Phys.*, **8**(20), 6003–6035, doi: [10.5194/acp-8-6003-2008](https://doi.org/10.5194/acp-8-6003-2008).
- Blossey, P. N., C. S. Bretherton, J. Cetrone, and M. Kharoutdinov 2007, Cloud-resolving model simulations of KWAJEX: Model sensitivities and comparisons with satellite and radar observations, *J. Atmos. Sci.*, **64**(5), 1488–1508, doi: [10.1175/JAS3982.1](https://doi.org/10.1175/JAS3982.1).
- Boucher, O., and U. Lohmann 1995, The sulfate-CCN-cloud albedo effect, *Tellus, Ser. B*, **47**(3), 281–300, doi: [10.1034/j.1600-0889.47.issue3.1.x](https://doi.org/10.1034/j.1600-0889.47.issue3.1.x).
- Bougiatioti, A., C. Fountoukis, N. Kalivitis, S. N. Pandis, A. Nenes, and N. Mihalopoulos 2009, Cloud condensation nuclei measurements in the marine boundary layer of the eastern Mediterranean: CCN closure and droplet growth kinetics, *Atmos. Chem. Phys.*, **9**(18), 7053–7066, doi: [10.5194/acp-9-7053-2009](https://doi.org/10.5194/acp-9-7053-2009).
- Bretherton, C. S., and S. Park 2009, A new moist turbulence parameterization in the community atmosphere model, *J. Clim.*, **22**(12), 3422–3448, doi: [10.1175/2008JCLI2556.1](https://doi.org/10.1175/2008JCLI2556.1).
- Chen, Y., and J. E. Penner 2005, Uncertainty analysis for estimates of the first indirect aerosol effect, *Atmos. Chem. Phys.*, **5**(11), 2935–2948, doi: [10.5194/acp-5-2935-2005](https://doi.org/10.5194/acp-5-2935-2005).
- Chen, W. T., Y. H. Lee, P. J. Adams, A. Nenes, and J. H. Seinfeld 2010a, Will black carbon mitigation dampen aerosol indirect forcing?, *Geophys. Res. Lett.*, **37**, L09801, doi: [10.1029/2010GL042886](https://doi.org/10.1029/2010GL042886).
- Chen, W. T., A. Nenes, H. Liao, P. J. Adams, J. L. F. Li, and J. H. Seinfeld 2010b, Global climate response to anthropogenic aerosol indirect effects: Present day and year 2100, *J. Geophys. Res.*, **115**, D12207, doi: [10.1029/2008JD011619](https://doi.org/10.1029/2008JD011619).
- Chuang, P. Y. 2003, Measurement of the timescale of hygroscopic growth for atmospheric aerosols, *J. Geophys. Res.*, **108**(D9), 4282., doi: [10.1029/2002JD002757](https://doi.org/10.1029/2002JD002757).
- Chuang, C. C., J. E. Penner, K. E. Taylor, S. Grossman, and J. J. Walton 1997, An assessment of the radiative effects of anthropogenic sulfate, *J. Geophys. Res.*, **102**(D3), 3761–3778, doi: [10.1029/96JD03087](https://doi.org/10.1029/96JD03087).
- Chuang, C. C., J. E. Penner, J. M. Prospero, K. E. Grant, G. H. Rau, and K. Kawamoto 2002, Cloud susceptibility and the first aerosol indirect forcing: Sensitivity to black carbon and aerosol concentrations, *J. Geophys. Res.*, **107**, 4564., doi: [10.1029/2000JD000215](https://doi.org/10.1029/2000JD000215).
- Clark, T. L. 1974, On modelling nucleation and condensation theory in Eulerian spatial domain, *J. Atmos. Sci.*, **31**, 2099–2117, doi: [10.1175/1520-0469\(1974\)031<2099:OMNACT>2.0.CO;2](https://doi.org/10.1175/1520-0469(1974)031<2099:OMNACT>2.0.CO;2).
- Cohard, J. M., J. P. Pinty, and C. Bedos 1998, Extending Twomey's analytical estimate of nucleated cloud droplet concentrations from CCN spectra, *J. Atmos. Sci.*, **55**(22), 3348–3357, doi: [10.1175/1520-0469\(1998\)055<3348:ETSABO>2.0.CO;2](https://doi.org/10.1175/1520-0469(1998)055<3348:ETSABO>2.0.CO;2).
- Cohard, J. M., J. P. Pinty, and K. Suhre 2000, On the parameterization of activation spectra from cloud condensation nuclei microphysical properties, *J. Geophys. Res.*, **105**(D9), 11,753–11,766, doi: [10.1029/1999JD901195](https://doi.org/10.1029/1999JD901195).
- Dearden, C. 2009, Investigating the simulation of cloud microphysical processes in numerical models using a

- one-dimensional dynamical framework, *Atmos. Sci. Lett.*, **10**, 207–214, doi: [10.1002/asl.239](https://doi.org/10.1002/asl.239).
- Engelhart, G. J., A. Asa-Awuku, A. Nenes, and S. N. Pandis 2008, CCN activity and droplet growth kinetics of fresh and aged monoterpene secondary organic aerosol, *Atmos. Chem. Phys.*, **8**(14), 3937–3949, doi: [10.5194/acp-8-3937-2008](https://doi.org/10.5194/acp-8-3937-2008).
- Engelhart, G. J., R. H. Moore, A. Nenes, and S. N. Pandis 2011, CCN activity of isoprene secondary organic aerosol, *J. Geophys. Res.*, **116**, D02207, doi: [10.1029/2010JD014706](https://doi.org/10.1029/2010JD014706).
- Ervens, B., A. G. Carlton, B. J. Turpin, K. E. Altieri, S. M. Kreidenweis, and G. Feingold 2008, Secondary organic aerosol yields from cloud-processing of isoprene oxidation products, *Geophys. Res. Lett.*, **35**, L02816, doi: [10.1029/2007GL031828](https://doi.org/10.1029/2007GL031828).
- Fan, J., R. Zhang, G. Li, W.-K. Tao, and X. Li 2007, Simulations of cumulus clouds using a spectral microphysics cloud-resolving model, *J. Geophys. Res.*, **112**, D04201, doi: [10.1029/2006JD007688](https://doi.org/10.1029/2006JD007688).
- Fan, J., T. Yuan, J. M. Comstock, S. Ghan, A. Khain, L. R. Leung, Z. Li, V. J. Martins, and M. Ovchinnikov 2009, Dominant role by vertical wind shear in regulating aerosol effects on deep convective clouds, *J. Geophys. Res.*, **114**, D22206, doi: [10.1029/2009JD012352](https://doi.org/10.1029/2009JD012352).
- Fitzgerald, J. W. 1974, Effect of aerosol composition on cloud droplet size distribution: A numerical study, *J. Atmos. Sci.*, **31**(5), 1358–1367, doi: [10.1175/1520-0469\(1974\)031<1358:EOACOC>2.0.CO;2](https://doi.org/10.1175/1520-0469(1974)031<1358:EOACOC>2.0.CO;2).
- Flossmann, A. I., W. D. Hall, and H. R. Pruppacher 1985, A theoretical study of the wet removal of atmospheric pollutants. 1. The redistribution of aerosol-particles captured through nucleation and impaction scavenging by growing cloud drops, *J. Atmos. Sci.*, **42**(6), 583–606, doi: [10.1175/1520-0469\(1985\)042<0583:ATSOTW>2.0.CO;2](https://doi.org/10.1175/1520-0469(1985)042<0583:ATSOTW>2.0.CO;2).
- Forster, P., et al., 2007, Changes in atmospheric constituents and in radiative forcing, in *Climate Change 2007: The Physical Science Basis. Contribution of Working Group I to the Fourth Assessment Report of the Intergovernmental Panel on Climate Change*, edited by S. Solomon et al., pp. 129–234, Cambridge Univ. Press, New York.
- Fountoukis, C., and A. Nenes 2005, Continued development of a cloud droplet formation parameterization for global climate models, *J. Geophys. Res.*, **110**, D11212, doi: [10.1029/2004JD005591](https://doi.org/10.1029/2004JD005591).
- Fountoukis, C., et al., 2007, Aerosol–cloud drop concentration closure for clouds sampled during the International Consortium for Atmospheric Research on Transport and Transformation 2004 campaign, *J. Geophys. Res.*, **112**, D10S30, doi: [10.1029/2006JD007272](https://doi.org/10.1029/2006JD007272).
- Fridlind, A., et al., 2004, Evidence for the predominance of mid-tropospheric aerosols as subtropical anvil cloud nuclei, *Science*, **304**(5671), 718–722, doi: [10.1126/science.1094947](https://doi.org/10.1126/science.1094947).
- Fuchs, N. A. 1959, *Evaporation and Droplet Growth in Gaseous Media*, Pergamon, New York.
- Fukuta, N., and L. A. Walter 1970, Kinetics of hydrometeor growth from a vapor-spherical model, *J. Atmos. Sci.*, **27**(8), 1160–1172, doi: [10.1175/1520-0469\(1970\)027<1160:KOHGFA>2.0.CO;2](https://doi.org/10.1175/1520-0469(1970)027<1160:KOHGFA>2.0.CO;2).
- Gottelman, A., H. Morrison, and S. J. Ghan 2008, A new two-moment bulk stratiform cloud microphysics scheme in the community atmosphere model, version 3 (CAM3). Part II: Single-column and global results, *J. Clim.*, **21**(15), 3660–3679, doi: [10.1175/2008JCLI2116.1](https://doi.org/10.1175/2008JCLI2116.1).
- Ghan, S. J., and R. C. Easter 2006, Impact of cloud-borne aerosol representation on aerosol direct and indirect effects, *Atmos. Chem. Phys.*, **6**(12), 4163–4174, doi: [10.5194/acp-6-4163-2006](https://doi.org/10.5194/acp-6-4163-2006).
- Ghan, S. J., C. C. Chuang, and J. E. Penner 1993, A parameterization of cloud droplet nucleation. Part I: Single aerosol type, *Atmos. Res.*, **30**, 198–221, doi: [10.1016/0169-8095\(93\)90024-I](https://doi.org/10.1016/0169-8095(93)90024-I).
- Ghan, S. J., C. C. Chuang, R. C. Easter, and J. E. Penner 1995, A parameterization of cloud droplet nucleation. Part II: Multiple aerosol types, *Atmos. Res.*, **36**, 39–54, doi: [10.1016/0169-8095\(94\)00005-X](https://doi.org/10.1016/0169-8095(94)00005-X).
- Ghan, S. J., L. R. Leung, R. C. Easter, and K. Abdul-Razzak 1997, Prediction of cloud droplet number in a general circulation model, *J. Geophys. Res.*, **102**(D18), 21,777–21,794, doi: [10.1029/97JD01810](https://doi.org/10.1029/97JD01810).
- Ghan, S. J., R. C. Easter, J. Hudson, and F.-M. Breon 2001a, Evaluation of aerosol indirect radiative forcing in MIRAGE, *J. Geophys. Res.*, **106**(D6), 5317–5334, doi: [10.1029/2000JD900501](https://doi.org/10.1029/2000JD900501).
- Ghan, S. J., et al., 2001b, A physically-based estimate of radiative forcing by anthropogenic sulfate aerosol, *J. Geophys. Res.*, **106**(D6), 5279–5293, doi: [10.1029/2000JD900503](https://doi.org/10.1029/2000JD900503).
- Guo, H., J. E. Penner, M. Herzog, and S. Xie 2007, Investigation of the first and second aerosol indirect effects using data from the May 2003 Intensive Operational Period at the southern Great Plains, *J. Geophys. Res.*, **112**, D15206, doi: [10.1029/2006JD007173](https://doi.org/10.1029/2006JD007173).
- Guo, H., J.-C. Golaz, L. J. Donner, V. E. Larson, D. P. Schanen, and B. M. Griffin 2010, Multi-variate probability density functions with dynamics for cloud droplet activation in large-scale models: Single column tests, *Geosci. Model Dev.*, **3**, 475–486, doi: [10.5194/gmd-3-475-2010](https://doi.org/10.5194/gmd-3-475-2010).
- Gustafson, W. I., E. G. Chapman, S. J. Ghan, R. C. Easter, and J. D. Fast 2007, Impact on modeled cloud characteristics due to simplified treatment of uniform cloud condensation nuclei during NEAQS 2004, *Geophys. Res. Lett.*, **34**, L19809, doi: [10.1029/2007GL030021](https://doi.org/10.1029/2007GL030021).
- Hänel, G. 1976, The properties of atmospheric aerosol particles as function of the relative humidity at thermodynamic equilibrium with the surrounding moist air,

- Adv. Geophys.*, **19**, 73–188, doi: [10.1016/S0065-2687\(08\)60142-9](https://doi.org/10.1016/S0065-2687(08)60142-9).
- Hänel, G. 1987, The role of aerosol properties during the condensational stage of cloud: A reinvestigation of numerics and microphysics, *Beitr. Phys. Atmos.*, **60**, 321–339.
- Haywood, J., and O. Boucher 2000, Estimates of the direct and indirect radiative forcing due to tropospheric aerosols: A review, *Rev. Geophys.*, **38**(4), 513–543, doi: [10.1029/1999RG000078](https://doi.org/10.1029/1999RG000078).
- Heymsfield, A. J., A. Bansemer, G. Heymsfield, and A. O. Fierro 2009, Microphysics of maritime tropical convective updrafts at temperatures from -20° to -60° , *J. Atmos. Sci.*, **66**(12), 3530–3562, doi: [10.1175/2009JAS3107.1](https://doi.org/10.1175/2009JAS3107.1).
- Hoose, C., J. E. Kristjánsson, T. Iversen, A. Kirkevåg, Ø. Seland, and A. Gettelman 2009, Constraining cloud droplet number concentration in GCMs suppresses the aerosol indirect effect, *Geophys. Res. Lett.*, **36**, L12807, doi: [10.1029/2009GL038568](https://doi.org/10.1029/2009GL038568).
- Hoppel, W. A., G. M. Frick, and R. E. Larson 1986, Effect of nonprecipitating clouds on the aerosol size distribution in the marine boundary-layer, *Geophys. Res. Lett.*, **13**(2), 125–128, doi: [10.1029/GL013i002p00125](https://doi.org/10.1029/GL013i002p00125).
- Howell, W. E. 1949, The growth of cloud drops in uniformly cooled air, *J. Meteorol.*, **6**(2), 134–149, doi: [10.1175/1520-0469\(1949\)006<0134:TGOCDI>2.0.CO;2](https://doi.org/10.1175/1520-0469(1949)006<0134:TGOCDI>2.0.CO;2).
- Hsieh, W. C. 2009, Representing droplet size distribution and cloud processes in aerosol-cloud-climate interaction studies, Ph.D. dissertation, Ga. Inst. of Technol., Atlanta.
- Ivanova, I. T., and H. G. Leighton 2008, Aerosol-cloud interactions in a mesoscale model. Part I: Sensitivity to activation and collision-coalescence, *J. Atmos. Sci.*, **65**(2), 289–308, doi: [10.1175/2007JAS2207.1](https://doi.org/10.1175/2007JAS2207.1).
- Jensen, J. B., and R. J. Charlson 1984, On the efficiency of nucleation scavenging, *Tellus, Ser. B*, **36**(5), 367–375, doi: [10.1111/j.1600-0889.1984.tb00255.x](https://doi.org/10.1111/j.1600-0889.1984.tb00255.x).
- Jones, A., and A. Slingo 1996, Predicting cloud-droplet effective radius and indirect sulphate aerosol forcing using a general circulation model, *Q. J. R. Meteorol. Soc.*, **122**, 1573–1595.
- Jones, A., D. L. Roberts, and A. Slingo 1994, A climate model study of indirect radiative forcing by anthropogenic sulphate aerosols, *Nature*, **370**, 450–453, doi: [10.1038/370450a0](https://doi.org/10.1038/370450a0).
- Khain, A., A. Pokrovsky, M. Pinsky, A. Seifert, and V. Phillips 2004, Simulation of effects of atmospheric aerosols on deep turbulent convective clouds using a spectral microphysics mixed-phase cumulus cloud model. Part I: Model description and possible applications, *J. Atmos. Sci.*, **61**(24), 2963–2982, doi: [10.1175/JAS-3350.1](https://doi.org/10.1175/JAS-3350.1).
- Khairoutdinov, M. F., and Y. L. Kogan 1999, A large eddy simulation model with explicit microphysics: Validation against aircraft observations of a stratocumulus-topped boundary layer, *J. Atmos. Sci.*, **56**(13), 2115–2131, doi: [10.1175/1520-0469\(1999\)056<2115:ALESMW>2.0.CO;2](https://doi.org/10.1175/1520-0469(1999)056<2115:ALESMW>2.0.CO;2).
- Khairoutdinov, M. F., and D. A. Randall 2003, Cloud resolving modeling of the ARM summer 1997 IOP: Model formulation, results, uncertainties, and sensitivities, *J. Atmos. Sci.*, **60**(4), 607–625, doi: [10.1175/1520-0469\(2003\)060<0607:CRMOTA>2.0.CO;2](https://doi.org/10.1175/1520-0469(2003)060<0607:CRMOTA>2.0.CO;2).
- Khvorostyanov, V. I., and J. A. Curry 2006, Aerosol size spectra and CCN activity spectra: Reconciling the log-normal, algebraic, and power laws, *J. Geophys. Res.*, **111**, D12202, doi: [10.1029/2005JD006532](https://doi.org/10.1029/2005JD006532).
- Khvorostyanov, V. I., and J. A. Curry 2008, Kinetics of cloud drop formation and its parameterization for cloud and climate models, *J. Atmos. Sci.*, **65**(9), 2784–2802, doi: [10.1175/2008JAS2606.1](https://doi.org/10.1175/2008JAS2606.1).
- Khvorostyanov, V. I., and J. A. Curry 2009, Parameterization of cloud drop activation based on analytical asymptotic solutions to the supersaturation equation, *J. Atmos. Sci.*, **66**(7), 1905–1925, doi: [10.1175/2009JAS2811.1](https://doi.org/10.1175/2009JAS2811.1).
- Kivekas, N., V. M. Kerminen, T. Anttila, H. Korhonen, H. Lihavainen, M. Komppula, and M. Kulmala 2008, Parameterization of cloud droplet activation using a simplified treatment of the aerosol number size distribution, *J. Geophys. Res.*, **113**, D15207, doi: [10.1029/2007JD009485](https://doi.org/10.1029/2007JD009485).
- Kogan, Y. L. 1991, The simulation of a convective cloud in a 3-D model with explicit microphysics. 1. Model description and sensitivity experiments, *J. Atmos. Sci.*, **48**(9), 1160–1189, doi: [10.1175/1520-0469\(1991\)048<1160:TSOACC>2.0.CO;2](https://doi.org/10.1175/1520-0469(1991)048<1160:TSOACC>2.0.CO;2).
- Köhler, H. 1921, Zur Kondensation des Wasserdampfe in der Atmosphäre, *Geophys. Publ.*, **2**, 3–15.
- Köhler, H. 1926, Zur Thermodynamic der Kondensation an hygroskopischen Kernen un Bemerkungen uber das Zusammenfließen der Tropfen, *Medd. Met. Hydro. Anst. Stockholm*, **3**(8).
- Korolev, A. V. 1994, A study of bimodal droplet size distributions in stratiform clouds, *Atmos. Res.*, **32**, 143–170, doi: [10.1016/0169-8095\(94\)90057-4](https://doi.org/10.1016/0169-8095(94)90057-4).
- Korolev, A. V. 1995, The influence of supersaturation fluctuations on droplet size spectra formation, *J. Atmos. Sci.*, **52**(20), 3620–3634, doi: [10.1175/1520-0469\(1995\)052<3620:TIOSFO>2.0.CO;2](https://doi.org/10.1175/1520-0469(1995)052<3620:TIOSFO>2.0.CO;2).
- Korolev, A. V., and I. P. Mazin 1993, Zones of increased and decreased droplet concentration in stratiform clouds, *J. Appl. Meteorol.*, **32**, 760–773, doi: [10.1175/1520-0450\(1993\)032<0760:ZOIADD>2.0.CO;2](https://doi.org/10.1175/1520-0450(1993)032<0760:ZOIADD>2.0.CO;2).
- Kreidenweis, S. M., et al., 2003, Modification of aerosol mass and size distribution due to aqueous-phase SO₂ oxidation in clouds: Comparisons of several models, *J. Geophys. Res.*, **108**(D7), 4213., doi: [10.1029/2002JD002697](https://doi.org/10.1029/2002JD002697).
- Kumar, P., A. Nenes, and I. Sokolik 2009a, The importance of adsorption for CCN activity and hygroscopic

- properties of mineral dust aerosol, *Geophys. Res. Lett.*, **36**, L24804, doi: [10.1029/2009GL040827](https://doi.org/10.1029/2009GL040827).
- Kumar, P., I. N. Sokolik, and A. Nenes 2009b, Parameterization of cloud droplet formation for global and regional models: Including adsorption activation from insoluble CCN, *Atmos. Chem. Phys.*, **9**(7), 2517–2532, doi: [10.5194/acp-9-2517-2009](https://doi.org/10.5194/acp-9-2517-2009).
- Kumar, P., I. N. Sokolik, and A. Nenes 2011a, Measurements of cloud condensation nuclei activity and droplet activation kinetics of fresh unprocessed regional dust samples and minerals, *Atmos. Chem. Phys.*, **11**(7), 3527–3541, doi: [10.5194/acp-11-3527-2011](https://doi.org/10.5194/acp-11-3527-2011).
- Kumar, P., I. N. Sokolik, and A. Nenes 2011b, Measurements of cloud condensation nuclei activity and droplet activation kinetics of wet processed regional dust samples and minerals, *Atmos. Chem. Phys. Discuss.*, **11**(4), 12,561–12,605, doi: [10.5194/acpd-11-12561-2011](https://doi.org/10.5194/acpd-11-12561-2011).
- Lance, S. 2007, Quantifying compositional impacts of ambient aerosol on cloud droplet formation, Ph.D. dissertation, Ga. Inst. of Technol., Atlanta.
- Latham, T. L., P. Kumar, A. Nenes, J. Dufek, I. N. Sokolik, M. Trail, and A. Russell 2011, Hygroscopic properties of volcanic ash, *Geophys. Res. Lett.*, **38**, L11802, doi: [10.1029/2011GL047298](https://doi.org/10.1029/2011GL047298).
- Leaitch, W. R., and G. A. Isaac 1994, On the relationship between sulfate and cloud droplet number concentration, *J. Clim.*, **7**, 206–212, doi: [10.1175/1520-0442\(1994\)007<0206:OTRBSA>2.0.CO;2](https://doi.org/10.1175/1520-0442(1994)007<0206:OTRBSA>2.0.CO;2).
- Leaitch, W. R., G. A. Isaac, J. W. Strapp, C. M. Banic, and H. A. Wiebe 1992, The relationship between cloud droplet number concentrations and anthropogenic pollution: Observations and climatic implications, *J. Geophys. Res.*, **97**(D2), 2463–2474.
- Lee, S. S., L. J. Donner, V. T. J. Phillips, and Y. Ming 2008a, Examination of aerosol effects on precipitation in deep convective clouds during the 1997 ARM summer experiment, *Q. J. R. Meteorol. Soc.*, **134**, 1201–1220, doi: [10.1002/qj.287](https://doi.org/10.1002/qj.287).
- Lee, S. S., L. J. Donner, V. T. J. Phillips, and Y. Ming 2008b, The dependence of aerosol effects on clouds and precipitation on cloud-system organization, shear and stability, *J. Geophys. Res.*, **113**, D16202, doi: [10.1029/2007JD009224](https://doi.org/10.1029/2007JD009224).
- Lee, S. S., J. E. Penner, and M. Wang 2009a, Comparison of a global-climate model simulation to a cloud-system resolving model simulation for long-term thin stratocumulus clouds, *Atmos. Chem. Phys.*, **9**(17), 6497–6520, doi: [10.5194/acp-9-6497-2009](https://doi.org/10.5194/acp-9-6497-2009).
- Lee, S. S., L. J. Donner, and V. T. J. Phillips 2009b, Sensitivity of aerosol and cloud effects on radiation to cloud types: Comparison between deep convective clouds and warm stratiform clouds over one-day period, *Atmos. Chem. Phys.*, **9**(7), 2555–2575, doi: [10.5194/acp-9-2555-2009](https://doi.org/10.5194/acp-9-2555-2009).
- Lee, S. S., L. J. Donner, and J. E. Penner 2010, Thunderstorm and stratocumulus: How does their contrasting morphology affect their interactions with aerosols?, *Atmos. Chem. Phys.*, **10**(14), 6819–6837, doi: [10.5194/acp-10-6819-2010](https://doi.org/10.5194/acp-10-6819-2010).
- Li, G., Y. Wang, and R. Zhang 2008, Implementation of a two-moment bulk microphysics scheme to the WRF model to investigate aerosol-cloud interaction, *J. Geophys. Res.*, **113**, D15211, doi: [10.1029/2007JD009361](https://doi.org/10.1029/2007JD009361).
- Lin, H., and W. R. Leaitch 1997, Development of an in-cloud aerosol activation parameterization for climate modelling, in *Proceedings of the WMO Workshop on Measurement of Cloud Properties for Forecasts of Weather, Air Quality and Climate*, pp. 328–335, World Meteorol. Organ., Geneva, Switzerland.
- Lohmann, U. 2008, Global anthropogenic aerosol effects on convective clouds in ECHAM5-HAM, *Atmos. Chem. Phys.*, **8**(7), 2115–2131, doi: [10.5194/acp-8-2115-2008](https://doi.org/10.5194/acp-8-2115-2008).
- Lohmann, U., and J. Feichter 1997, Impact of sulfate aerosols on albedo and lifetime of clouds: A sensitivity study with the ECHAM4 GCM, *J. Geophys. Res.*, **102**(D12), 13,685–13,700, doi: [10.1029/97JD00631](https://doi.org/10.1029/97JD00631).
- Lohmann, U., and J. Feichter 2005, Global indirect aerosol effects: A review, *Atmos. Chem. Phys.*, **5**(3), 715–737, doi: [10.5194/acp-5-715-2005](https://doi.org/10.5194/acp-5-715-2005).
- Lohmann, U., and S. Ferrachat 2010, Impact of parametric uncertainties on the present-day climate and on the anthropogenic aerosol effect, *Atmos. Chem. Phys.*, **10**(23), 11,373–11,383, doi: [10.5194/acp-10-11373-2010](https://doi.org/10.5194/acp-10-11373-2010).
- Lohmann, U., J. Feichter, C. C. Chuang, and J. E. Penner 1999, Prediction of the number of cloud droplets in the ECHAM GCM, *J. Geophys. Res.*, **104**(D8), 9169–9198, doi: [10.1029/1999JD900046](https://doi.org/10.1029/1999JD900046).
- Lohmann, U., J. Feichter, J. E. Penner, and W. R. Leaitch 2000, Indirect effect of sulfate and carbonaceous aerosols: A mechanistic treatment, *J. Geophys. Res.*, **105**(D10), 12,193–12,206, doi: [10.1029/1999JD901199](https://doi.org/10.1029/1999JD901199).
- Lohmann, U., P. Stier, C. Hoose, S. Ferrachat, S. Kloster, E. Roeckner, and J. Zhang 2007, Cloud microphysics and aerosol indirect effects in the global climate model ECHAM5-HAM, *Atmos. Chem. Phys.*, **7**(13), 3425–3446, doi: [10.5194/acp-7-3425-2007](https://doi.org/10.5194/acp-7-3425-2007).
- Lohmann, U., et al., 2010, Total aerosol effect: Radiative forcing or radiative flux perturbation? *Atmos. Chem. Phys.*, **10**(7), 3235–3246, doi: [10.5194/acp-10-3235-2010](https://doi.org/10.5194/acp-10-3235-2010).
- Luo, Y. L., K. M. Xu, H. Morrison, and G. McFarquhar 2008, Arctic mixed-phase clouds simulated by a cloud-resolving model: Comparison with ARM observations and sensitivity to microphysics parameterizations, *J. Atmos. Sci.*, **65**(4), 1285–1303, doi: [10.1175/2007JAS2467.1](https://doi.org/10.1175/2007JAS2467.1).
- Magaritz, L., M. Pinsky, A. P. Khain, and O. Krasnov 2009, Investigation of droplet size distributions and drizzle formation using a new trajectory ensemble model. Part

- 2: Lucky parcels in non-mixing limit, *J. Atmos. Sci.*, **66**(4), 781–805, doi: [10.1175/2008JAS2789.1](https://doi.org/10.1175/2008JAS2789.1).
- Martin, G. M., G. W. Johnson, and A. Spice 1994, The measurement and parameterization of effective radius of droplets in warm stratocumulus clouds, *J. Atmos. Sci.*, **51**(13), 1823–1842, doi: [10.1175/1520-0469\(1994\)051<1823:TMAPOE>2.0.CO;2](https://doi.org/10.1175/1520-0469(1994)051<1823:TMAPOE>2.0.CO;2).
- Mason, B. J., and C. W. Chien 1962, Cloud-droplet growth by condensation in cumulus, *Q. J. R. Meteorol. Soc.*, **88**, 136–142, doi: [10.1002/qj.49708837603](https://doi.org/10.1002/qj.49708837603).
- Meng, Z. Y., and J. H. Seinfeld 1994, On the source of the submicrometer droplet mode of urban and regional aerosols, *Aerosol Sci. Technol.*, **20**(3), 253–265, doi: [10.1080/02786829408959681](https://doi.org/10.1080/02786829408959681).
- Menon, S., and L. Rotstayn 2006, The radiative influence of aerosol effects on liquid-phase cumulus and stratiform clouds based on sensitivity studies with two climate models, *Clim. Dyn.*, **27**, 345–356, doi: [10.1007/s00382-006-0139-3](https://doi.org/10.1007/s00382-006-0139-3).
- Meskhidze, N., A. Nenes, W. C. Conant, and J. H. Seinfeld 2005, Evaluation of a new cloud droplet activation parameterization with in situ data from CRYSTAL-FACE and CSTRIFE, *J. Geophys. Res.*, **110**, D16202, doi: [10.1029/2004JD005703](https://doi.org/10.1029/2004JD005703).
- Ming, Y., V. Ramaswamy, L. J. Donner, and V. T. J. Phillips 2006, A new parameterization of cloud droplet activation applicable to general circulation models, *J. Atmos. Sci.*, **63**(4), 1348–1356, doi: [10.1175/JAS3686.1](https://doi.org/10.1175/JAS3686.1).
- Ming, Y., V. Ramaswamy, L. J. Donner, V. T. J. Phillips, S. A. Klein, P. A. Ginoux, and L. W. Horowitz 2007, Modeling the interactions between aerosols and liquid water clouds with a self-consistent cloud scheme in a general circulation model, *J. Atmos. Sci.*, **64**(4), 1189–1209, doi: [10.1175/JAS3874.1](https://doi.org/10.1175/JAS3874.1).
- Moore, R. H., E. D. Ingall, A. Sorooshian, and A. Nenes 2008, Molar mass, surface tension, and droplet growth kinetics of marine organics from measurements of CCN activity, *Geophys. Res. Lett.*, **35**, L07801, doi: [10.1029/2008GL033350](https://doi.org/10.1029/2008GL033350).
- Morales, R., and A. Nenes 2010, Characteristic updrafts for computing distribution-averaged cloud droplet number and stratocumulus cloud properties, *J. Geophys. Res.*, **115**, D18220, doi: [10.1029/2009JD013233](https://doi.org/10.1029/2009JD013233).
- Morrison, H., and A. Gettelman 2008, A new two-moment bulk stratiform cloud microphysics scheme in the Community Atmosphere Model, version 3 (CAM3). Part I: Description and numerical tests, *J. Clim.*, **21**, 3642–3659, doi: [10.1175/2008JCLI2105.1](https://doi.org/10.1175/2008JCLI2105.1).
- Morrison, H., and W. Grabowski 2008, Modeling supersaturation and subgrid-scale mixing with two-moment bulk warm microphysics, *J. Atmos. Sci.*, **65**(3), 792–812, doi: [10.1175/2007JAS2374.1](https://doi.org/10.1175/2007JAS2374.1).
- Morrison, H., J. A. Curry, and V. I. Khvorostyanov 2005, A new double-moment microphysics parameterization for application in cloud and climate models. Part I: Description, *J. Atmos. Sci.*, **62**(6), 1665–1677, doi: [10.1175/JAS3446.1](https://doi.org/10.1175/JAS3446.1).
- Morrison, H., J. O. Pinto, J. A. Curry, and G. M. McFarquhar 2008, Sensitivity of modeled arctic mixed-phase stratocumulus to cloud condensation and ice nuclei over regionally varying surface conditions, *J. Geophys. Res.*, **113**, D05203, doi: [10.1029/2007JD008729](https://doi.org/10.1029/2007JD008729).
- Mozurkewich, M. 1986, Aerosol growth and the condensation coefficient for water: A review, *Aerosol Sci. Technol.*, **5**(2), 223–236, doi: [10.1080/02786828608959089](https://doi.org/10.1080/02786828608959089).
- Murphy, S. M., et al., 2009, comprehensive simultaneous shipboard and airborne characterization of exhaust from a modern container ship at sea, *Environ. Sci. Technol.*, **43**(13), 4626–4640, doi: [10.1021/es802413j](https://doi.org/10.1021/es802413j).
- Nenes, A., and J. H. Seinfeld 2003, Parameterization of cloud droplet formation in global climate models, *J. Geophys. Res.*, **108**(D14), 4415, doi: [10.1029/2002JD002911](https://doi.org/10.1029/2002JD002911).
- Nenes, A., S. Ghan, H. Abdul-Razzak, P. Y. Chuang, and J. H. Seinfeld 2001, Kinetic limitations on cloud droplet formation and impact on cloud albedo, *Tellus, Ser. B*, **53**(2), 133–149, doi: [10.1034/j.1600-0889.2001.d01-12.x](https://doi.org/10.1034/j.1600-0889.2001.d01-12.x).
- Nenes, A., R. J. Charlson, M. C. Facchini, M. Kulmala, A. Laaksonen, and J. H. Seinfeld 2002, Can chemical effects on cloud droplet number rival the first indirect effect?, *Geophys. Res. Lett.*, **29**(17), 1848, doi: [10.1029/2002GL015295](https://doi.org/10.1029/2002GL015295).
- Ovtchinnikov, M., and S. J. Ghan 2005, Parallel simulations of aerosol influence on clouds using a cloud-resolving model and a single column model, *J. Geophys. Res.*, **110**, D15S10, doi: [10.1029/2004JD005088](https://doi.org/10.1029/2004JD005088).
- Padro, L. T., D. Tkacik, T. Latham, C. J. Hennigan, A. P. Sullivan, R. J. Weber, L. G. Huey, and A. Nenes 2010, Investigation of cloud condensation nuclei properties and droplet growth kinetics of the water-soluble aerosol fraction in Mexico City, *J. Geophys. Res.*, **115**, D09204, doi: [10.1029/2009JD013195](https://doi.org/10.1029/2009JD013195).
- Park, S., and C. S. Bretherton 2009, The University of Washington shallow convection and moist turbulence schemes and their impact on climate simulations with the community atmosphere model, *J. Clim.*, **22**(12), 3449–3469, doi: [10.1175/2008JCLI2557.1](https://doi.org/10.1175/2008JCLI2557.1).
- Penner, J. E., et al., 2006, Model intercomparison of indirect aerosol effects, *Atmos. Chem. Phys.*, **6**(11), 3391–3405, doi: [10.5194/acp-6-3391-2006](https://doi.org/10.5194/acp-6-3391-2006).
- Perri, M. J., S. Seitzinger, and B. J. Turpin 2009, Secondary organic aerosol production from aqueous photooxidation of glycolaldehyde: Laboratory experiments, *Atmos. Environ.*, **43**(8), 1487–1497, doi: [10.1016/j.atmosenv.2008.11.037](https://doi.org/10.1016/j.atmosenv.2008.11.037).
- Petters, M. D., and S. M. Kreidenweis 2007, A single parameter representation of hygroscopic growth and cloud condensation nucleus activity, *Atmos. Chem. Phys.*, **7**(8), 1961–1971, doi: [10.5194/acp-7-1961-2007](https://doi.org/10.5194/acp-7-1961-2007).

- Pinsky, M. B., and A. P. Khain 2002, Effects of in-cloud nucleation and turbulence on droplet spectrum formation in cumulus clouds, *Q. J. R. Meteorol. Soc.*, **128**, 501–533, doi: [10.1256/003590002321042072](https://doi.org/10.1256/003590002321042072).
- Pringle, K. J., K. S. Carslaw, D. V. Spracklen, G. M. Mann, and M. P. Chipperfield 2009, The relationship between aerosol and cloud drop number concentrations in a global aerosol microphysics model, *Atmos. Chem. Phys.*, **9**(12), 4131–4144, doi: [10.5194/acp-9-4131-2009](https://doi.org/10.5194/acp-9-4131-2009).
- Pruppacher, H. R., and J. D. Klett 1997, *Microphysics of Clouds and Precipitation*, Kluwer Acad., Norwell, Mass.
- Quaas, J., et al., 2009, Aerosol indirect effects general circulation model intercomparison and evaluation with satellite data, *Atmos. Chem. Phys.*, **9**(22), 8697–8717, doi: [10.5194/acp-9-8697-2009](https://doi.org/10.5194/acp-9-8697-2009).
- Rasch, P. J., M. C. Barth, J. T. Kiehl, S. E. Schwartz, and C. M. Benkovitz 2000, A description of the global sulfur cycle and its controlling processes in the National Center for Atmospheric Research Community Climate Model, Version 3, *J. Geophys. Res.*, **105**(D5), 6783., doi: [10.1029/2000JD900036](https://doi.org/10.1029/2000JD900036).
- Rissman, T. A., A. Nenes, and J. H. Seinfeld 2004, Chemical amplification (or dampening) of the Twomey effect: Conditions derived from droplet activation theory, *J. Atmos. Sci.*, **61**(8), 919–930, doi: [10.1175/1520-0469\(2004\)061<0919:CAODOT>2.0.CO;2](https://doi.org/10.1175/1520-0469(2004)061<0919:CAODOT>2.0.CO;2).
- Roelofs, G. J., P. Stier, J. Feichter, E. Vignati, and J. Wilson 2006, Aerosol activation and cloud processing in the global aerosol-climate model ECHAM5-HAM, *Atmos. Chem. Phys.*, **6**(9), 2389–2399, doi: [10.5194/acp-6-2389-2006](https://doi.org/10.5194/acp-6-2389-2006).
- Ruehl, C. R., P. Y. Chuang, and A. Nenes 2008, How quickly do cloud droplets form on atmospheric particles?, *Atmos. Chem. Phys.*, **8**(4), 1043–1055, doi: [10.5194/acp-8-1043-2008](https://doi.org/10.5194/acp-8-1043-2008).
- Ruehl, C. R., P. Y. Chuang, and A. Nenes 2009, Distinct CCN activation kinetics above the marine boundary layer along the California coast, *Geophys. Res. Lett.*, **36**, L15814, doi: [10.1029/2009GL038839](https://doi.org/10.1029/2009GL038839).
- Russell, L. M., and J. H. Seinfeld 1998, Size- and composition-resolved externally mixed aerosol model, *Aerosol Sci. Technol.*, **28**(5), 403–416, doi: [10.1080/02786829808965534](https://doi.org/10.1080/02786829808965534).
- Saleeby, S. M., and W. R. Cotton 2004, Large-droplet mode and prognostic number concentration of cloud droplets in the Colorado State University Regional Atmospheric Modeling System (RAMS). Part I: Module descriptions and supercell test simulations, *J. Appl. Meteorol.*, **43**, 182–195, doi: [10.1175/1520-0450\(2004\)043<0182:ALMAPN>2.0.CO;2](https://doi.org/10.1175/1520-0450(2004)043<0182:ALMAPN>2.0.CO;2).
- Salzmann, M., Y. Ming, J. C. Golaz, P. Ginoux, H. Morrison, A. Gettelman, M. Kramer, and L. J. Donner 2010, Two-moment bulk stratiform cloud microphysics in the GFDL AM3 GCM: Description, evaluation, and sensitivity tests, *Atmos. Chem. Phys.*, **10**(16), 8037–8064, doi: [10.5194/acp-10-8037-2010](https://doi.org/10.5194/acp-10-8037-2010).
- Segal, Y., and A. Khain 2006, Dependence of droplet concentration on aerosol conditions in different cloud types: Application to droplet concentration parameterization of aerosol conditions, *J. Geophys. Res.*, **111**, D15204, doi: [10.1029/2005JD006561](https://doi.org/10.1029/2005JD006561).
- Segal, Y., M. Pinsky, A. Khain, and C. Erlick 2003, Thermodynamic factors influencing bimodal spectrum formation in cumulus clouds, *Atmos. Res.*, **66**, 43–64, doi: [10.1016/S0169-8095\(02\)00172-2](https://doi.org/10.1016/S0169-8095(02)00172-2).
- Seinfeld, J. H., and S. N. Pandis 1998, *Atmospheric Chemistry and Physics: From Air Pollution to Climate Change*, John Wiley, Hoboken, N. J.
- Seland, Ø., T. Iversen, A. Kirkevåg, and T. Storelvmo 2008, Aerosol-climate interactions in the CAM-Oslo atmospheric GCM and investigation of associated basic shortcomings, *Tellus, Ser. A*, **60**(3), 459–491, doi: [10.1111/j.1600-0870.2008.00318.x](https://doi.org/10.1111/j.1600-0870.2008.00318.x).
- Shantz, N. C., R. Y. W. Chang, J. G. Slowik, A. Vlasenko, J. P. D. Abbatt, and W. R. Leaitch 2010, Slower CCN growth kinetics of anthropogenic aerosol compared to biogenic aerosol observed at a rural site, *Atmos. Chem. Phys.*, **10**(1), 299–312, doi: [10.5194/acp-10-299-2010](https://doi.org/10.5194/acp-10-299-2010).
- Shi, X. 2010, Cloud microphysics and aerosol indirect effects in the grid-point atmospheric model of IAP LASG (GAMIL), Ph.D. dissertation, Chin. Acad. of Sci., Beijing.
- Shima, S., K. Kusano, A. Kawano, T. Sugiyama, and S. Kawahara 2009, The super-droplet method for the numerical simulation of clouds and precipitation: A particle-based and probabilistic microphysics model coupled with a non-hydrostatic model, *Q. J. R. Meteorol. Soc.*, **135**, 1307–1320, doi: [10.1002/qj.441](https://doi.org/10.1002/qj.441).
- Shipway, B. J., and S. J. Abel 2010, Analytical estimation of cloud droplet nucleation based on an underlying aerosol population, *Atmos. Res.*, **96**, 344–355, doi: [10.1016/j.atmosres.2009.10.005](https://doi.org/10.1016/j.atmosres.2009.10.005).
- Solomos, S., G. Kallos, J. Kushta, M. Astitha, C. Tremback, A. Nenes, and Z. Levin 2011, An integrated modeling study on the effects of mineral dust and sea salt particles on clouds and precipitation, *Atmos. Chem. Phys.*, **11**(2), 873–892, doi: [10.5194/acp-11-873-2011](https://doi.org/10.5194/acp-11-873-2011).
- Song, X., and G. J. Zhang 2011, Microphysics parameterization for convective clouds in a global climate model, Part I: Description and single-column model tests, *J. Geophys. Res.*, **116**, D02201, doi: [10.1029/2010JD014833](https://doi.org/10.1029/2010JD014833).
- Sorooshian, A., M. L. Lu, F. J. Brechtel, H. Jonsson, G. Feingold, R. C. Flagan, and J. H. Seinfeld 2007, On the source of organic acid aerosol layers above clouds, *Environ. Sci. Technol.*, **41**(13), 4647–4654, doi: [10.1021/es0630442](https://doi.org/10.1021/es0630442).
- Sorooshian, A., et al., 2008, Comprehensive airborne characterization of aerosol from a major bovine source, *Atmos. Chem. Phys.*, **8**(17), 5489–5520, doi: [10.5194/acp-8-5489-2008](https://doi.org/10.5194/acp-8-5489-2008).

- Sotiropoulou, R. E. P., A. Nenes, P. J. Adams, and J. H. Seinfeld 2007, Cloud condensation nuclei prediction error from application of Köhler theory: Importance for the aerosol indirect effect, *J. Geophys. Res.*, **112**, D12202, doi: [10.1029/2006JD007834](https://doi.org/10.1029/2006JD007834).
- Stevens, B., and G. Feingold 2009, Untangling aerosol effects on clouds and precipitation in a buffered system, *Nature*, **461**(7264), 607–613, doi: [10.1038/nature08281](https://doi.org/10.1038/nature08281).
- Stevens, B., R. L. Walko, W. R. Cotton, and G. Feingold 1996, Spurious production of cloud-edge supersaturations by Eulerian models, *Mon. Weather Rev.*, **124**(5), 1034–1041, doi: [10.1175/1520-0493\(1996\)124<1034:TSPOCE>2.0.CO;2](https://doi.org/10.1175/1520-0493(1996)124<1034:TSPOCE>2.0.CO;2).
- Storelvmo, T., J. E. Kristjansson, S. J. Ghan, A. Kirkevåg, O. Seland, and T. Iversen 2006, Predicting cloud droplet number concentration in Community Atmosphere Model (CAM)-Oslo, *J. Geophys. Res.*, **111**, D24208, doi: [10.1029/2005JD006300](https://doi.org/10.1029/2005JD006300).
- Storelvmo, T., J. E. Kristjansson, U. Lohmann, T. Iversen, A. Kirkevåg, and Ø. Seland 2008, Modeling of the Wegener–Bergeron–Findeisen process—Implications for aerosol indirect effects, *Environ. Res. Lett.*, **3**, 045001, doi: [10.1088/1748-9326/3/4/045001](https://doi.org/10.1088/1748-9326/3/4/045001).
- Sud, Y. C., et al., 2009, Sensitivity of boreal-summer circulation and precipitation to atmospheric aerosols in selected regions—Part 1: Africa and India, *Ann. Geophys.*, **27**(10), 3989–4007, doi: [10.5194/angeo-27-3989-2009](https://doi.org/10.5194/angeo-27-3989-2009).
- Takemura, T., T. Nozawa, S. Emori, T. Y. Nakajima, and T. Nakajima 2005, Simulation of climate response to aerosol direct and indirect effects with aerosol transport-radiation model, *J. Geophys. Res.*, **110**, D02202, doi: [10.1029/2004JD005029](https://doi.org/10.1029/2004JD005029).
- Twomey, S. 1959, The nuclei of natural cloud formation. Part II: The supersaturation in natural clouds and the variation of droplet concentration, *Pure Appl. Geophys.*, **43**, 243–249, doi: [10.1007/BF01993560](https://doi.org/10.1007/BF01993560).
- Twomey, S. 1974, Pollution and planetary albedo, *Atmos. Environ.*, **8**(12), 1251–1256, doi: [10.1016/0004-6981\(74\)90004-3](https://doi.org/10.1016/0004-6981(74)90004-3).
- Twomey, S. 1977, Influence of pollution on shortwave albedo of clouds, *J. Atmos. Sci.*, **34**(7), 1149–1152, doi: [10.1175/1520-0469\(1977\)034<1149:TIOPOT>2.0.CO;2](https://doi.org/10.1175/1520-0469(1977)034<1149:TIOPOT>2.0.CO;2).
- Wang, M., and J. E. Penner 2009, Aerosol indirect forcing in a global model with particle nucleation, *Atmos. Chem. Phys.*, **9**(1), 239–260, doi: [10.5194/acp-9-239-2009](https://doi.org/10.5194/acp-9-239-2009).
- Wang, M., et al., 2011a, The multi-scale aerosol-climate model PNNL-MMF: model description and evaluation, *Geosci. Model Dev.*, **4**, 137–168, doi: [10.5194/gmd-4-137-2011](https://doi.org/10.5194/gmd-4-137-2011).
- Wang, M., et al., 2011b, Aerosol indirect effects in a multi-scale aerosol-climate model PNNL-MMF, *Atmos. Chem. Phys.*, **11**, 5431–5455, doi: [10.5194/acp-11-5431-2011](https://doi.org/10.5194/acp-11-5431-2011).
- Warner, J. 1973, The microstructure of cumulus cloud: Part IV. The effect on the droplet spectrum of mixing between cloud and environment, *J. Atmos. Sci.*, **30**(2), 256–261, doi: [10.1175/1520-0469\(1973\)030<0256:TMOCCP>2.0.CO;2](https://doi.org/10.1175/1520-0469(1973)030<0256:TMOCCP>2.0.CO;2).
- Westervelt, D. M., R. H. Moore, A. Nenes, and P. J. Adams 2011, Effect of primary organic sea spray emissions on cloud condensation nuclei concentrations, *Atmos. Chem. Phys. Discuss.*, **11**(2), 5757–5784, doi: [10.5194/acpd-11-5757-2011](https://doi.org/10.5194/acpd-11-5757-2011).
- Whitby, K. T. 1978, Physical characteristics of sulfur aerosols, *Atmos. Environ.*, **12**(1–3), 135–159, doi: [10.1016/0004-6981\(78\)90196-8](https://doi.org/10.1016/0004-6981(78)90196-8).
- Xue, H., and G. Feingold 2006, Large-eddy simulations of trade wind cumuli: Investigation of aerosol indirect effects, *J. Atmos. Sci.*, **63**(6), 1605–1622, doi: [10.1175/JAS3706.1](https://doi.org/10.1175/JAS3706.1).
- Yuter, S. E., R. A. Houze, E. A. Smith, T. T. Wilheit, and E. Zipser 2005, Physical characterization of tropical oceanic convection observed in KWAJEX, *J. Appl. Meteorol.*, **44**(4), 385–415, doi: [10.1175/JAM2206.1](https://doi.org/10.1175/JAM2206.1).

Appendix A: Symbols

The Kelvin coefficient is defined

$$A \equiv \frac{4M_w \sigma}{RT \rho_w} \quad (\text{A1})$$

where M_w is the molecular weight of water, σ is the surface tension (assumed to be that of water unless surfactants are present), R the ideal gas constant for water vapor, T temperature, and ρ_w the density of liquid water.

The hygroscopicity parameter for a particle composed of a mixture of soluble and insoluble components can be expressed [Hänel, 1976; Pruppacher and Klett, 1997; Abdul-Razzak and Ghan, 2000; Petters and Kreidenweis, 2007] as the volume mean of the hygroscopicity of each component,

$$k \equiv \frac{\sum_j q_j k_j / \rho_j}{\sum_j q_j / \rho_j} \quad (\text{A2})$$

where

$$k_j \equiv \frac{\rho_j M_w v_j \varepsilon_j}{\rho_w M_j} \quad (\text{A3})$$

is the hygroscopicity of component j comprising the particle, M_j is the molecular weight of the solute component j , ρ_j the density of component j , q_j the mass fraction of component j , v_j the number of ions the solute component dissociates into, and ε_j is the soluble fraction of component j

in the dry particle. For an internal mixture of soluble and insoluble components, all particles are assumed to have the same composition, so (A2) describes the hygroscopicity of the mixture of components, with q_j the mass mixing ratio of component j . *Petters and Kreidenweis [2007]* show that the volume mixing rule accurately determines the hygroscopicity of an internal mixture of components with very different hygroscopicities.

The growth coefficient is defined [*Pruppacher and Klett, 1997; Seinfeld and Pandis, 1998*]

$$G \equiv \left(\frac{\rho_w RT}{e_s D'_v M_w} + \frac{L \rho_w}{K'_v T} \left(\frac{LM_w}{RT} - 1 \right) \right)^{-1} \quad (\text{A4})$$

where e_s is the saturation vapor pressure of water, L is the latent heat of vaporization of water, and the modified vapor diffusivity and thermal conductivity depend on droplet size [*Fukuta and Walter, 1970; Fitzgerald, 1974*]:

$$D'_v \equiv \frac{D_v}{\frac{r}{r + \Delta_v} + \frac{D_v}{\alpha_c r} \left(\frac{2\pi M_w}{RT} \right)^{1/2}} \quad (\text{A5})$$

$$K'_a \equiv \frac{K_a}{\frac{r}{r + \Delta_T} + \frac{K_a}{\alpha_T r \rho c_p} \left(\frac{2\pi M_w}{RT} \right)^{1/2}} \quad (\text{A6})$$

where D_v and K_a are the diffusivity of water vapor and the thermal conductivity of air [*Pruppacher and Klett, 1997; Seinfeld and Pandis, 1998*], Δ_v and Δ_T are the vapor and temperature jump lengths [*Fuchs, 1959; Fitzgerald, 1974; Pruppacher and Klett, 1997*], α_c is the condensation coefficient [*Mozurkewich, 1986*], and α_T is the thermal accommodation coefficient.

In addition,

$$\alpha \equiv \frac{g M_w L}{c_p R T^2} - \frac{g M_a}{RT} \quad (\text{A7})$$

$$\gamma \equiv \frac{p M_a}{e_s M_w} + \frac{M_w L^2}{c_p R T^2} \quad (\text{A8})$$

where g is acceleration due to gravity, p is atmospheric pressure, M_a is the molecular weight of dry air, and c_p is the specific heat of air.